A promoter polymorphism defines distinct roles in anther development for Col-0 and Ler-0 alleles of Arabidopsis *ACYL-COA BINDING PROTEIN3*

Ze-Hua Guo[1] (iD), **Tai-Hua Hu**[1] (iD), **Mohd Fadhli Hamdan**[1] (iD), **Minghui Li**[2] (iD), **Ruifeng Wang**[2] (iD), **Jie Xu**[2,3] (iD), **Shiu-Cheung Lung**[1] (iD), **Wanqi Liang**[2,4] (iD), **Jianxin Shi**[2,4] (iD), **Dabing Zhang**[2,4] (iD) and **Mee-Len Chye**[1] (iD)

[1]School of Biological Sciences, The University of Hong Kong, Pokfulam, Hong Kong, China; [2]Joint International Research Laboratory of Metabolic & Developmental Sciences, State Key Laboratory of Hybrid Rice, School of Life Sciences and Biotechnology, Shanghai Jiao Tong University, Shanghai, 200240, China; [3]The Core Facility and Service Center (CFSC), School of Life Sciences and Biotechnology, Shanghai Jiao Tong University, Shanghai, 200240, China; [4]Yazhou Bay Institute of Deepsea Sci-Tech, Shanghai Jiao Tong University, Sanya, 572024, China

Authors for correspondence:
Ze-Hua Guo
Email: gzh90thu@connect.hku.hk

Mee-Len Chye
Email: mlchye@hku.hk

Summary

- Acyl-CoA-Binding Proteins (ACBPs) bind acyl-CoA esters and function in lipid metabolism. Although *acbp3-1*, the *ACBP3* mutant in *Arabidopsis thaliana* ecotype Col-0, displays normal floral development, the *acbp3-2* mutant from ecotype Ler-0 characterized herein exhibits defective adaxial anther lobes and improper sporocyte formation.

- To understand these differences and identify the role of ERECTA in ACBP3 function, the *acbp3* mutants and *acbp3-erecta* (*er*) lines were analyzed by microscopy for anther morphology and high-performance liquid chromatography for lipid composition.

- Defects in Landsberg anther development were related to the ERECTA-mediated pathway because the progenies of *acbp3-2* × La-0 and *acbp3-1* × *er-1* in Col-0 showed normal anthers, contrasting to that of *acbp3-2* in Ler-0. Polymorphism in the regulatory region of *ACBP3* enabled its function in anther development in Ler-0 but not Col-0 which harbored an AT-repeat insertion. *ACBP3* expression and anther development in *acbp3-2* were restored using *ACBP3pro (Ler)::ACBP3* not *ACBP3pro (Col)::ACBP3*. SPOROCYTELESS (SPL), a sporocyte formation regulator activated *ACBP3* transcription in Ler-0 but not Col-0.

- For anther development, the ERECTA-related role of *ACBP3* is required in Ler-0, but not Col-0. The disrupted promoter regulatory region for SPL binding in Col-0 eliminates the role of *ACBP3* in anther development.

Introduction

Acyl-CoA-binding proteins (ACBPs), present in eukaryotes and some prokaryotes (Burton *et al.*, 2005; Xiao & Chye, 2011a; Du *et al.*, 2016; Lung & Chye, 2016; Ye & Chye, 2016), have versatile functions in plant reproduction (Chen *et al.*, 2010; Zheng *et al.*, 2012; Du *et al.*, 2013a,b; Ye *et al.*, 2016, 2017; Guo *et al.*, 2019a,b, 2022; Fadhli Hamdan *et al.*, 2022) as well as in stress responses and signaling (Chen *et al.*, 2008, 2018; Gao *et al.*, 2009; Du *et al.*, 2010, 2013b; Liao *et al.*, 2014; Hu *et al.*, 2018; Panthapulakkal Narayanan *et al.*, 2019; Guo *et al.*, 2021; Lung *et al.*, 2022). They are a family of proteins conserved at the acyl-CoA-binding domain which binds acyl-CoA thioesters. ACBPs maintain intracellular acyl-CoA pools and transport acyl-CoA thioesters in lipid metabolism (Xiao & Chye, 2011a; Du *et al.*, 2016; Lung & Chye, 2016; Ye & Chye, 2016).

In *Arabidopsis thaliana*, all six *ACBPs* are expressed in flowers (Zheng *et al.*, 2012; Du *et al.*, 2013a,b; Ye *et al.*, 2016).

However, only *ACBP2*, *ACBP4* and *ACBP5* are expressed in the anthers (Du *et al.*, 2013b; Hsiao *et al.*, 2015; Ye *et al.*, 2017). Although the expression of *ACBP2pro (Col)::GUS* was detected in pollen grains, the precise role of *ACBP2* in anther development remains to be elucidated (Du *et al.*, 2013b). *ACBP4*, *ACBP5* and *ACBP6* have been implicated in floral development (Hsiao *et al.*, 2015; Ye *et al.*, 2017) because the accumulation of cuticular waxes and cutin monomers in *acbp4*, *acbp5* and *acbp4 acbp5* mutant flower buds was altered in comparison to the Col-0 wild-type (WT) (Ye *et al.*, 2017). Additionally, knockout of *ACBP4*, *ACBP5* and *ACBP6* resulted in reduced pollen grain numbers (Hsiao *et al.*, 2015). In flower buds, stearic acid content declined in *acbp4* while linolenic acid increased in *acbp4 acbp5* in comparison to the WT (Ye *et al.*, 2017). Furthermore, upregulation of *ACBP5* was observed in *acbp4* inflorescence while upregulation of *ACBP4* was seen in *acbp5* inflorescences (Ye *et al.*, 2017), suggesting a collaborative role for these two kelch-motif-containing ACBPs in lipid metabolism throughout floral

development. While the functions of ACBP4, ACBP5 and ACBP6 in flowers have been identified, less is known on the function of ACBP3 in plant reproduction despite its reported floral expression (Zheng et al., 2012).

In Col-0 flowers, *ACBP3pro (Col)::GUS* expression was observed in the stigmata whereas *ACBP4pro (Col)::GUS* and *ACBP5pro (Col)::GUS* were expressed in anthers (Zheng et al., 2012). Besides detection in the flowers, *ACBP3pro (Col)::GUS* was found in the phloem tissues of Arabidopsis rosettes and roots (Zheng et al., 2012). Previous studies on *ACBP3* have mainly been focused on the vegetative tissues rather than the reproductive tissues of Col-0 (Xiao et al., 2010; Hu et al., 2018). Subcellular localization experiments in both transient and stable transformants revealed that ACBP3 is localized to both the endoplasmic reticulum and Golgi membranes as well as the extracellular matrix (Leung et al., 2006; Xiao et al., 2010). Overexpression of *ACBP3* not only conferred protection against *Pseudomonas syringae* DC 3000 (Xiao & Chye, 2011b) but also induced early leaf senescence (Xiao et al., 2010). Depletion of ACBP3 in *acbp3-1* of Col-0 resulted in higher levels of 12:0- and 14:0-fatty acid (FA) content but lower 18:2-FA, 18:3-FA and methyl jasmonate content in the phloem (Hu et al., 2018), suggesting a potential role for ACBP3 in binding fatty-acyl-CoA-thioesters in the phloem. Gaining a deeper understanding of ACBP functions in plant reproduction may provide valuable insights into the molecular processes regulating organ development that ultimately influence fruit and seed formation. Furthermore, as ACBPs are highly-conserved proteins, investigations into the role of plant ACBPs can enhance our understanding on the evolution and conservation of ACBPs across different ecotypes and species. Studies on ACBPs in various ecotypes may provide an important context for understanding genetic variation and adaptation that facilitates phenotypic variability among Arabidopsis ecotypes.

While Col-0 is the most extensively studied Arabidopsis genotype with its genome sequenced (AGI, 2000), other ecotypes have also been utilized (Kowalski et al., 1994; Kunkel, 1996; Crawford & Yanofsky, 2011; Schmalenbach et al., 2014). Among these ecotypes, Landsberg *erecta*-0 (L*er*-0) harbors a loss-of-function mutation in the gene *ERECTA*, resulting in a compact and firm inflorescence appearance (Rédei, 1962; Torii et al., 1996). The gene functions of the *ERECTA* family members including *ERECTA*, *ERECTA-LIKE1* (*ERL1*), and *ERL2* have been extensively studied given the impact of the *erecta* (*er*) mutation (Pillitteri et al., 2007; Hord et al., 2008; van Zanten et al., 2009). Owing to its convenient handling facilitated by the compact inflorescence phenotype, L*er*-0 has become a popular genetic background for mutant analyses and studies on natural variation (van Zanten et al., 2009).

The work presented here demonstrates that *acbp3-2* (a knock-out mutant of *ACBP3* in L*er*-0) but not *acbp3-1* (a knock-out mutant of *ACBP3* in Col-0) exhibits defective development of adaxial anther lobes. The new observations on the *acbp3-2* mutant from L*er*-0 prompted us to compare it with our past Col-0 *acbp3-1* mutant (Xiao et al., 2010) to address the role of ACBP3 in reproduction. The observed phenotypic differences in anther development were not solely attributed to ERECTA, but

involved regulatory polymorphism in the promoter region of *ACBP3* between L*er*-0 and Col-0. Under the regulation of *SPOROCYTELESS* (*SPL*), *ACBP3pro (Ler)::ACBP3::GFP*, but not *ACBP3pro (Col)::ACBP3::GFP*, showed high expression in anthers and rescued aberrant adaxial anther lobe formation. Additionally, acyl-CoA composition in both *acbp3-2* mutant and *spl* mutant anthers varied significantly from that of the L*er*-0 control. This study identified promoter polymorphism regulating *ACBP3* floral expression, the role of ACBP3 in acyl-CoA metabolism and anther development.

Materials and Methods

Plant materials and growth conditions

Arabidopsis thaliana Col-0, Landsberg-0 (La-0) and L*er*-0 were used in this study. Besides, Kn-0, Ws-2, Van-0, Edi-0, Ull2-3, Tottarp-2, Ws-0, St-0, Ct-0, Cvi-0, Oy-0 and Ge-0 were also included for RNA analysis in flower buds. All of the 15 *Arabidopsis* WTs were obtained from the Arabidopsis Biological Resource Center (ABRC). Arabidopsis seeds were surface-sterilized in solution containing 1.25% (w/v) sodium hypochlorite and 0.1% (v/v) Triton X-100. Seeds were subsequently rinsed in sterilized double distilled H$_2$O (ddH$_2$O) and placed on to Murashige & Skoog medium (Murashige & Skoog, 1962). Stratification of seeds was carried out at 4°C in the dark for 3 d, followed by germination of seeds at 22°C with 16 h of light. Ten-day-old seedlings were potted in soil and grown at 23°C : 21°C, day : night cycles with 16 h of light.

The *er-1* mutant refers to Arabidopsis Col-0 mutant stock CS3378 (Lease et al., 2001; Abraham et al., 2013). The *acbp3-2* mutant from L*er*-0 was crossed with the *er-1* mutant from Col-0 to generate *acbp3-2 er-1* double mutant hybrid plants. The resulting F$_1$ plants were subsequently self-fertilized to produce F$_2$ plants. The T-DNA insertions on *ACBP3* genomic sequence were confirmed from both chromosomes of F$_2$ plants by PCR-genotyped using ML348/A3CdsRev primers, and the verified F$_2$ plants were sampled for semithin sections under light microscopy. The *acbp3-1 × er-1* plants were generated by crossing *acbp3-1* and *er-1* mutant plants, and the F$_2$ homozygous plants were sampled for semithin sections under light microscopy. The *acbp3-2 × La-0* plants was made by crossing the *acbp3-2* mutant and La-0 WT plants, and the F$_2$ *acbp3-2* homozygous plants with *ERECTA*-complementation were sampled for semithin sections under light microscopy.

Characterization of *acbp3* mutants

The *acbp3-2* transposon mutant (stock no. At_5.12107, ecotype L*er*-0) and *acbp3-1* T-DNA mutant (stock no. SALK_012290, ecotype Col-0) seeds were provided by the Arabidopsis Information Resource (TAIR). The *acbp3-1* mutant in Col-0 was identified and characterized by Xiao et al. (2010) using PCR, RT-PCR and western blotting, while *acbp3-2* was identified with Southern blot and western blot analyses in this study. Southern blot analysis was conducted to determine copy numbers of insertion in transgenic Arabidopsis *acbp3-2* plants following Chye (1998) with

modifications as stated below. *Eco*RI-digested plant genomic DNA was separated and blotted to a Hybond-N membrane (Amersham, Slough, UK) according to the manufacturer. A DNA probe corresponding to the gene encoding neomycin phosphotransferase II (NPT II) in the *Ds* transposon insertion was labeled with DIG DNA Labeling Kit (Roche). The membrane was hybridized with DIG-labeled probes and developed using CDP-Star, ready-to-use (Roche) according to the manufacturer's instructions. Western blot analysis using anti-ACBP3 antibodies was carried out as according to the procedures used in the characterization of *acbp3-1* from Col-0 as described in Xiao *et al.* (2010).

The CRISPR-Cas9 construct for *ACBP3* gene knockout (*At4g24230*) was designed and the *ACBP3*-CRISPR line (*acbp3-3*) was generated in L*er*-0 by Edgene Biotechnology Co. Ltd, located in Wuhan, China. Seeds obtained from hygromycin (Hyg)-resistant transformants were further cultivated on half-strength MS plates supplemented with Hyg. Subsequently, T_2 homozygous plants were identified and verified through DNA sequencing.

For the generation of the *ACBP3* complemented lines, *ACBP3* genomic DNA from L*er*-0 (COM-L) and Col-0 (COM-C) were used. The 3.1-kb *ACBP3pro::ACBP3* fragments were PCR-amplified with primers ML3546/ML3547 (Supporting Information Table S1) using genomic DNA from L*er*-0 and Col-0, respectively. The amplicons were subsequently cloned into the *Bam*HI site on a transformation vector pCAMBIA1301-GFP (CAMBIA) with a Hyg-selectable marker (Liu *et al.*, 2020). The resultant constructs, pAT1088 harboring *ACBP3pro (Ler):: ACBP3::GFP* and pAT1089 harboring *ACBP3pro (Col):: ACBP3::GFP*, were respectively mobilized into *Agrobacterium tumefaciens* and introduced into the *acbp3-2* mutant by floral dip (Clough & Bent, 1998). The T_0 generation was selected using Hyg (50 mg l^{-1}) and the putative positive T_1 transformant was confirmed by PCR analysis using primers eGFP-pREUR-F and NOS-R (Table S1).

Microscopy analyses

Scanning electron microscopy (SEM) was performed according to Hord *et al.* (2008) with modifications at the fixation process. Flower buds and inflorescences were fixed with Formalin-Aceto-Alcohol (FAA) solution for 18 h at room temperature, followed by graded EtOH dehydration steps (50%, 70%, 90% and 100%) and a critical-point-drying (Bray *et al.*, 1993). Samples were then coated with a thin layer (100–200 Å) of metallic film, mounted on an adhesive stub, and observed under a scanning electron microscope LEO 1530 FEG (Zeiss).

For histochemical analyses, flower buds and inflorescences were fixed and dehydrated similarly as for SEM but were embedded in Technovit 7100 resin (Kulzer, South Bend, IN, USA) according to Yeung & Chan (2015). Three-micrometer cross-sections were generated using a Leica RM2135 microtome (Leica Biosystems, Nußloch, Germany), before staining with 0.5% (w/v) Toluidine Blue O followed by observation under fluorescence microscopy (Nikon 80i fluorescence microscope equipped with a Nikon DS-RI2 camera from Nikon Instruments, Tokyo, Japan). Floral developmental stages were based on Sanders *et al.* (1999).

For confocal microscopy analyses, Arabidopsis anthers were separated from the flowers, and images were obtained by confocal laser scanning microscopy using a Leica SP8 system. Fluorescence was excited at 514 nm and collected with a 500–550 nm filter. The resultant images were analyzed with IMAGEJ (Schneider *et al.*, 2012).

RNA analysis

TRIzol reagent (Invitrogen) was used for extraction of total RNA from 0.1 g of homogenized Arabidopsis bud samples. Subsequently, the total RNA was reverse-transcribed using the Superscript First-strand Synthesis System (Invitrogen) according to the manufacturer. Quantitative real-time PCR was conducted on a StepOne Plus Real-time PCR system using SYBR Green Mix (Applied Biosystems, Foster City, CA, USA) programmed as follows: 10 min at 95°C followed by 40 cycles of 95°C (15 s) and 56°C (1 min). For each reaction, three experimental replicates were performed with gene-specific primers (Table S1), and *ACTIN2* was used as a reference gene for normalization. Quantitative values were obtained using the delta delta Ct (ΔΔCt) method.

Lipid profiling

Acyl-CoAs were extracted from anthers following the method described by Haslam & Larson (2021). Briefly, Arabidopsis bud tissue was homogenized and mixed with 200 μl of extraction buffer containing isopropanol/50 mM KH_2PO_4/50 mg ml^{-1} BSA (25 : 25 : 1, v/v/v) acidified with glacial acetic acid, and 17:0-CoA added as an internal standard. The samples were then derivatized to chloroacetaldehyde derivatives by adding 200 μl 0.5 M chloroacetaldehyde in 0.15 M citric acid buffer (trisodium citrate/citric acid; pH 4.0), and 0.5% (w/v) SDS, followed by heating at 80°C for 30 min. Acyl-CoAs were separated using a 25-cm × 4.6-mm phenyl-hexyl Luna column (5-μm particle size; Phenomenex, Macclesfield, Cheshire, UK) and detected by fluorescence (λ_{ex} 230 nm/λ_{em} 420 nm) using an Agilent 1260 Infinity HPLC system with DAD/FLD (Agilent Technologies, Santa Clara, CA, USA).

Fatty acid analysis was conducted following Carvalho & Malcata (2005) with modifications as stated below. Arabidopsis flower buds were homogenized, and the powder dissolved in a transmethylation solution containing 1 ml of toluene, 2 ml of 1% (v/v) sulphuric acid in methanol together with 5 μl of an internal standard (C19:0 (1 mg ml^{-1} hexane)). The transmethylation solution of total FAs was injected into an Agilent 6890N equipped with a 5973 Mass Selective Detector (MSD) and a 30 m × 0.250 mm DB-WAX column (0.25 μm in film thickness) for data collection and analysis following Guo *et al.* (2019a).

Generation of *ACBP3pro (Ler)::GUS* transgenic plants in L*er*-0

ACBP3pro (Col)::GUS plants were first reported by Zheng *et al.* (2012). For the production of *ACBP3pro (Ler)::GUS* plants, a 1.7-kb fragment of the *ACBP3* 5′-flanking sequence was first amplified from Arabidopsis L*er*-0 DNA with primers

ML809/ML810 (Table S1) and subsequently cloned into pGEM-T Easy vector (Promega) to generate plasmid pAT1045. To construct the *ACBP3pro (Ler)::GUS* fusion, the 1.7-kb fragment of *ACBP3pro (Ler)* was then excised from plasmid pAT1045 using *Bam*HI and *Sma*I and cloned into similar sites of the *GUS*-containing vector pBI101.3 (Clontech, Mountain View, CA, USA) to generate the plant transformation vector pAT1046. The pAT1046-tranformed derivative of *A. tumefaciens* strain GV3101 (Zheng *et al.*, 2012) was then used to transform wild-type *A. thaliana* Ler-0 by the floral dip method (Clough & Bent, 1998). T_0 seeds were screened on MS medium containing kanamycin (50 μg ml^{-1}). Kanamycin-resistant T_1 transformants were subsequently verified by PCR using primer pair ML2916 and ML2917 (Table S1). PCR-verified T_3 transgenic plant lines were collected for GUS assays.

GUS assays

Histochemical GUS assays were carried out according to Jefferson *et al.* (1987). The flowers from various developmental stages as defined in Sanders *et al.* (1999) were submerged in a GUS substrate solution (100 mM sodium phosphate buffer pH 7.0, 1 mg ml^{-1} 5-bromo-4-chloro-3-indolyl-b-D-glucuronide, 2 mM potassium ferricyanide, 2 mM potassium ferrocyanide, 0.1% (v/v) triton X-100) and vacuum-infiltrated for 1 h, followed by 3-h incubation at 37°C. Subsequently, samples were cleared with 0.1% chloral hydrate (Sigma-Aldrich Inc.) and photographed with an Olympus SZX16 stereomicroscope (Olympus Corp., Tokyo, Japan). Images were then analyzed using a Nis-Elements Viewer (Nikon) and ImageJ software (Schneider *et al.*, 2012).

RNA *in situ* hybridization

Arabidopsis Ler-0 flower buds was fixed in FAA solution, comprised of 10% formaldehyde, 50% ethanol (EtOH) and 5% acetic acid in water, for 24 h at 4°C, followed by dehydration with graded EtOH solutions (70%, 85%, 95% and absolute EtOH) and embedment in paraffin according to Li *et al.* (2006). For generation of the antisense probe, the template for the antisense probe was amplified with primer pair A3ISH1T7-F/A3ISH1-R (Table S1), while A3ISH1T7-R/A3ISH1-F (Table S1) was utilized for the sense control using Arabidopsis Ler-0 flower buds cDNA as template in PCR. Digoxigenin (DIG)-labeled probes transcribed with the T7 promoter using the DIG RNA labelling kit (Roche), were employed in hybridization on 6-μm sections excised using a Leica microtome (RM2235) placed on microscopic slides. Dewaxing of sections, probe hybridization and immunological detection of DIG were performed as described in Kouchi & Hata (1993) with modifications as stated. Images were obtained using a Nikon microscope (Eclipse 80i).

Phylogenic analysis

ACBP3 5′-flanking sequences of representative Arabidopsis ecotypes including Ler-0, Kn-0, Col-0, Ws-2, Van-0, Edi-0, Ull2-3, Tottarp-2, Ws-0, St-0, Ct-0, Cvi-0, Oy-0 and Ge-0 were acquired from https://1001genomes.org/. An evolutionary study was carried out on the −1343/−1193 region at the *ACBP3* 5′-flanking sequences, and the sequences were aligned with the Muscle alignment program (Edgar, 2004a,b) at https://www.ebi.ac.uk/Tools/msa/muscle/ using the default parameter values. Phylogenetic analysis was performed using maximum likelihood methods with W-IQ-Tree 1.6.12 (Trifinopoulos *et al.*, 2016), and the model K3Pu+F+I was selected for the optimal tree by the Bayesian information criterion (Schwarz, 1978). The supporting value for each clade was estimated from 1000 bootstrap (Felsenstein, 1985) and 1000 SH-aLRT replicates (Anisimova & Gascuel, 2006). The tree was visualized using FigTree 1.4.4.

Electrophoretic mobility-shift assays (EMSAs)

The full-length cDNA of *AtSPL* was cloned into vector *pGADT7* (Clontech, TaKaRa, Shiga, Japan) to generate plasmid pAT1087 for *in vitro* transcription/translation to produce a HA-tagged recombinant protein using the TNT T7/SP6 Coupled Wheat Germ Extract System (Promega). Fluorescein amidite (FAM)-labeled probes were generated by annealing two complementary primers containing FAM at the 5′-end. The binding reaction mixture contained 25 mM Tris-acetate (pH 7.5), 1 mM DTT, 0.1 mg ml^{-1} BSA, 2 mM MgAc, 20 nM FAM-labeled DNA, and 3 μl of *in vitro* synthesized protein. The binding reaction was performed for 30 min at 25°C before loading on a 6% native polyacrylamide gel. Competition was tested using 10-fold excess of non-labeled probes. FAM-labeled probes were visualized using the FAM channel of a ChemiDoc MP imaging system (Bio-Rad). The primers are listed in Table S1; ML3540/ML3541, ML3542/ML3543 and ML3544/ML3545 were used to generate Probes 1, 2 and 3 of Ler-0, respectively and ML3548/ML3549, ML3550/ML3551 and ML3552/ML3553 for Probes 1, 2 and 3 of Col-0, respectively.

Luciferase assays

Luciferase (LUC) *trans*-activation assays were performed in *Nicotiana benthamiana* leaves, following Tao *et al.* (2018). Plasmid pREUR-EF (Liu *et al.*, 2020) was used as the effector vector. Plasmid pAT1078 was generated by introducing the cDNA sequence of *SPL* into pREUR-EF. Primers ML3524 and ML3525 are listed in Table S1. In the pREUR-EF derivative, the *SPL* cDNA is driven by an enhanced *35S* promoter, while the empty vector pREUR-EF was used as a negative control. Plasmid p0801 was modified from pGreenII 0800-LUC (Hellens *et al.*, 2005) to act as the reporter vector. The reporter plasmids harboring *ACBP3pro::LUC* were constructed by introducing the 1.7-kp *ACBP3* 5′-flanking sequence from each of Col-0 and Ler-0 to plasmid p0801 to drive the cDNA of firefly luciferase (FLUC). Primers ML3487/ML3488 (Table S1) were used to amplify the *ACBP3* 5′-flanking sequence from Col-0 and Ler-0.

Effectors and reporters were introduced with various combinations into *A. tumefaciens* GV3101, and then agroinfiltrated into 28-d old *N. benthamiana* leaves following Li *et al.* (2014). After 36-h incubation in the dark, the leaves were detached from the plants and swabbed with VivoGlo™ Luciferin, *In Vivo* Grade

(Promega), and pictures were captured by a cooling CCD imaging apparatus (Tanon 5200; Tianneng Life Science, Shanghai, China). Meanwhile, round-disk samples from *N. benthamiana* leaves were homogenized in liquid nitrogen. FLUC and *Renilla* luciferase (RLUC) activities were measured using the Dual-Luciferase® Reporter (DLR™) Assay System (Promega). The FLUC : RLUC ratio was measured in a GloMax 20/20 luminometer (Promega). Four biological replicates were used for each experiment.

Accession numbers

Sequence data from this article can be found in the TAIR (Arabidopsis) databases under accession nos.: *ACBP2* (AT4G27780), *ACBP3* (At4g24230), *SPL* (At4g27330), *EMS1* (At5g07280), *TPD1* (At4g24972), *AMS* (At2g16910), *MYB33* (At5g06100).

Results

Knockout of *ACBP3* impairs anther development in Arabidopsis Landsberg *erecta*-0

To examine the role of *ACBP3* in L*er*-0 anther development, Arabidopsis *acbp3* mutants were analyzed. Light microscopy analysis of semithin cross-sections from anthers of an *acbp3* Ds insertional mutant (Stock no. AT_5.12107) in L*er*-0, referred to as *acbp3-2* thereafter, revealed the presence of only two abaxial lobes and the absence of two adaxial lobes in these anthers (Fig. 1). This defect was not observed in the *acbp3-2* anthers until stage 4 of anther development (Fig. 1c). In comparison to the four-lobed anthers from L*er*-0 (Fig. 1d), the staged-4 *acbp3-2* anther possessed only two normal lobes (Fig. 1e). The development of its adaxial lobes failed at stage 3, leading to a lack of normal sporocyte formation (Fig. 1e). Additionally, the 'notch' representing the stomium region became visible only from stage 5 ('Str' in Fig. 1g). Cell differentiation in its adaxial lobes was disrupted from stage 3 as there were merely two layers of cells representing the epidermis and endothecium in the adaxial lobes of *acbp3-2* at stage 4 (Fig. 1e) in comparison to multiple layers in L*er*-0 (Fig. 1f).

To verify the roles of *ACBP3* in anther development as observed in L*er*-0, an additional *acbp3*-CRISPR line (referred to as *acbp3-3* thereafter) was generated in L*er*-0 and characterized genetically together with *acbp3-2*, followed by phenotypic analysis (Fig. 2). The insertion in the *acbp3-2* mutant was mapped to the first exon of *ACBP3*, and DNA sequence analysis showed the occurrence of a 94-bp deletion within the first exon of *ACBP3* in the *acbp3-3* (Figs 2a, S1A). Southern blot analysis using a probe for the *Ds* insertion confirmed the presence of a single insertion in the *acbp3-2* genome (Fig. S1B). Western blot analysis on rosettes using anti-ACBP3 antibodies (Xiao *et al.*, 2010) verified knockout of ACBP3 expression in *acbp3-2* as well as *acbp3-3* (Fig. S1C). Light microscopy on semithin cross-sections of *acbp3-2* and *acbp3-3* revealed that anthers at stages 7–9 from these two *acbp3* mutant lines lack the two adaxial lobes in comparison to L*er*-0 (Fig. 2c,d). In contrast, examination of the previously identified *acbp3-1* mutant in Col-0 (Xiao *et al.*, 2010)

did not reveal any defect in anther lobes (Fig. S2). To investigate whether *ERECTA* contributed to the distinct phenotypes observed between *acbp3* mutants in L*er*-0 and Col-0, crosses were performed using the *acbp3-2* mutant, the *er* mutant in Col-0 (*er-1*) and Arabidopsis La-0 WT. Anthers from the *acbp3-2 er-1* double mutant hybrid plants were normal in morphology for all four lobes (Fig. 2e), similar to *acbp3-1 × er-1* double mutant plants (Fig. 2f) and *acbp3-2 ×* La-0 plants (Fig. 2g), indicating that ERECTA modulates ACBP3 function differently in Landsberg and Columbia. In contrast to the anther phenotype of *acbp3-2*, the inflorescence morphology and vegetative growth of *acbp3-2* plants did not differ from L*er*-0 (Fig. S3). Similarly, the inflorescence morphology and vegetative growth of *acbp3-1* plants resembled those of Col-0 (Fig. S3). Taken together, the mutation of *ACBP3* in L*er*-0 (*acbp3-2*) but not Col-0 (*acbp3-1*) adversely impacts anther adaxial lobe development.

Null mutation in *ACBP3* affects lipid metabolism in flowers

Given the observed phenotypic change in the *acbp3-2* anthers, the lipid content in flower buds of *acbp3-2* and L*er*-0, and the acyl-CoA thioesters in anthers of various mutants (including *acbp3-1*, *acbp3-2*, *acbp3-3*, *acbp3-1 × er-1*, *acbp3-2 ×* La-0, *er-1* and *spl*) and L*er*-0/Col-0 were determined. Gas chromatography–mass spectrometry (GC-MS) results revealed that the flower bud FA composition of *acbp3-2* differs significantly from L*er*-0 (Fig. S4). Specifically, C16:3-, C18:2- and C18:3-FAs were remarkably lower in *acbp3-2* while C16:0-, C16:1-, C18:0-, and C18:1-FAs were significantly higher than L*er*-0 (Fig. S4). High-performance liquid chromatography (HPLC) data demonstrated that in comparison to the Col-0 control, the 10:0- and 18:3-CoA content in anthers of both *acbp3-1* and *er-1* mutants as well as the *acbp3-1 × er-1* plants declined (Fig. 3a), while 16:0-, 18:1- and 18:2-CoA composition in *acbp3-1 × er-1* plants rose (Fig. 3a). In contrast, HPLC results showed that in L*er*-0, 10:0-, 18:2- and 18:3-CoA content in anthers of *acbp3-2* and *acbp3-3* were lower than the L*er*-0 control, while levels of all acyl-CoA thioesters determined in anthers of the ACBP3-complemented line COM-L did not differ from the control (Fig. 3b). Interestingly, an *spl* mutant in L*er*-0 exhibited defective anther lobes (Yang *et al.*, 1999) similar to the deformed lobes of the *acbp3-2* mutants (Fig. 1). Levels of 10:0- and 18:3-CoA in anthers of *spl* were lower than L*er*-0 (Fig. 3b), and 10:0- and 18:2-CoA content in anthers of *acbp3-2 ×* La-0 plants also declined (Fig. 3b). Overall, the *acbp3* mutation *acbp3-1* decreased 10:0- and 18:3-CoA content in Col-0, while the *acbp3* mutations, *acbp3-2* and *acbp3-3*, reduced 10:0-, 18:2- and 18:3-CoA content in L*er*-0.

Genetic polymorphism at the *ACBP3* promoter affects its expression in developing anthers of Arabidopsis L*er*-0

Given that ACBP3 has not been reported to influence anther development in Col-0 (Fadhli Hamdan *et al.*, 2022), a comparison was made between the expression of *ACBP3* in floral tissue from L*er*-0 and Col-0. Histochemical β-glucuronidase (GUS) assays conducted on *ACBP3pro (Ler)::GUS* transgenic lines in Arabidopsis L*er*-0 showed signals in the developing anthers at stages 4–9 and in the
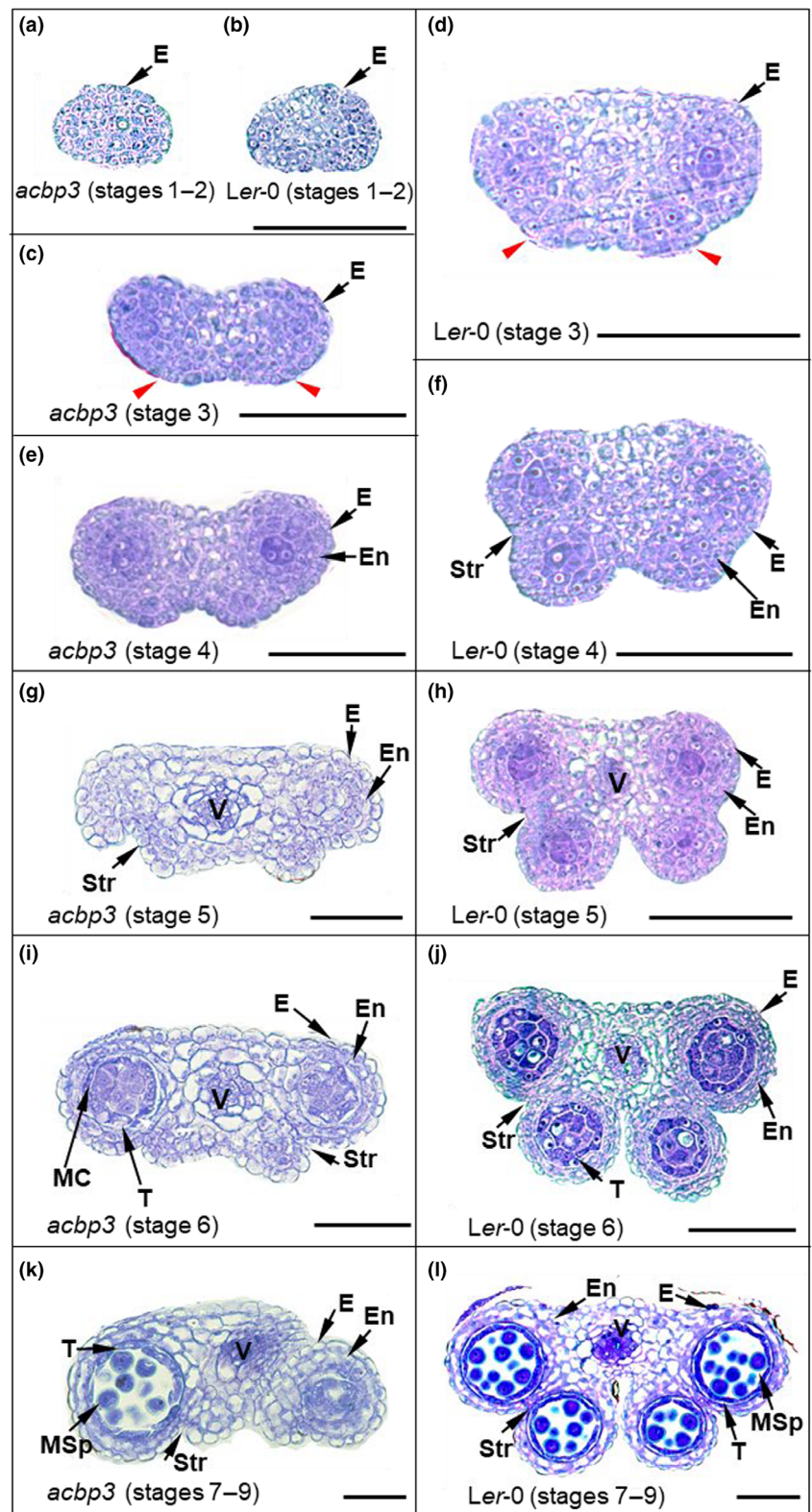
Fig. 1 Semithin-section analysis reveals abnormal lobe development in *Arabidopsis thaliana* ecotype L*er*-0 *acbp3-2* anthers. Developing anthers in *acbp3-2* (a, c, e, g, i, k) and L*er*-0 (b, d, f, h, j, l) are presented at stages 1–2 in (a, b), stage 3 in (c, d), stage 4 in (e, f), stage 5 in (g, h), stage 6 in (i, j), and stages 7–9 in (k, l), respectively. Red arrowheads indicate the positions in the *acbp3-2* anther that lacks the bottom two lobes (c) in comparison to similar positions in L*er*-0 at stage 3 (d). The abnormal adaxial lobes in (g, i, k) failed to form sporocytes. E, epidermis; En, endothecium; MC, meiotic cell; MSp, microspores; Str, stomium region; T, tapetum; V, vascular region. Bars: (a, b) 20 μm; (other panels) 50 μm. Representative pictures shown after three biological repeats.

stigma at stage 13 (Fig. 4). In contrast, analysis on *ACBP3pro (Col)::GUS* expression in Col-0 revealed strong GUS signals in the stigma and transmitting tract after stage 11, but not the anthers (Fig. S5), which is consistent with microarray data from TAIR and previous GUS staining results on fully-open Col-0 flowers (Zheng *et al.*, 2012). The differential expression of *ACBP3* prompted a comparison of their 5′-flanking sequences in Col-0 and L*er*-0. Alignment of the *ACBP3* 5′-flanking region sequence (data from https://1001genomes.org/) demonstrated major variations occurred at *c.* −1200 bp, 5′ of the transcription start site (+1), frequently
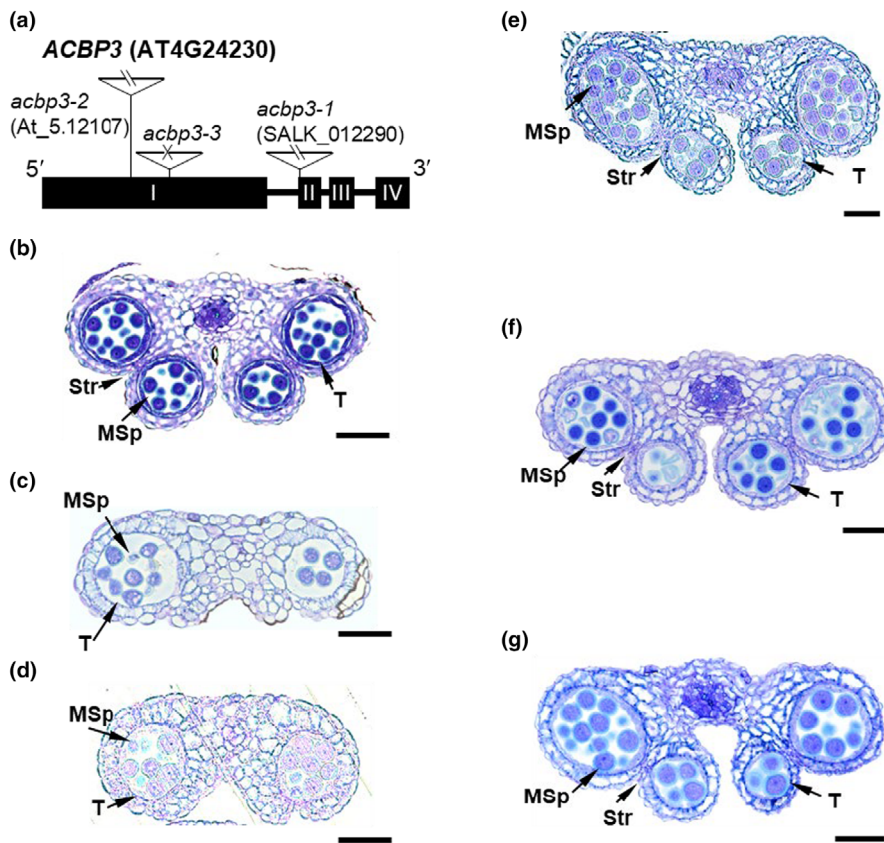
Fig. 2 Knockout of *ACBP3* in *Arabidopsis thaliana* ecotype L*er*-0 impairs anther development. (a) Schematic representation of *ACBP3* (AT4G24230) in ecotype L*er*-0. Black boxes represent exons (numbered in Roman numerals), and lines between them indicate introns. T-DNA insertion location in *acbp3-1* (SALK_012290) *acbp3-2* (At_5_12107) is marked by a triangle, and the *acbp3*-CRISPR (*acbp3-3*) deletion region by a crossed triangle. Semithin-sections of anthers staged 7–9 from L*er*-0 (b), *acbp3-2* (c), *acbp3-3* (d), the *acbp3-2* × *er-1* (Col) hybrid plant (e), the *acbp3-1* × *er-1* (f) in *Col-0* plant and the *acbp3-2* × La-0 plants (g). MSp, microspores; Str, stomium region; T, tapetum. Bars: (b–g) 50 μm. Pictures were taken from three biological repeats, and representative pictures are presented.

between −1343 and −1193 bp (data not shown). Further examination of *ACBP3* expression across 14 Arabidopsis ecotypes including L*er*-0, Kn-0, Col-0, Ws-2, Van-0, Edi-0, Ull2-3, Tottarp-2, Ws-0, St-0, Ct-0, Cvi-0, Oy-0 and Ge-0 revealed significantly higher levels of *ACBP3* expression specifically in L*er*-0 (Fig. S6).

To explore the mechanistic aspect of the observed higher expression of *ACBP3* in L*er*-0, an evolutionary tree on this region across those 14 Arabidopsis ecotypes was constructed to display the distances amongst various ecotypes. L*er*-0 and Col-0 showed relatively distant *ACBP3* 5′-flanking sequences (Fig. 5a). Further alignment of genomic DNA sequences from Col-0 and L*er*-0 identified promoter polymorphism, including 14 single nucleotide polymorphisms (SNPs) and one indel, located between −1343 and −1193 bp (Fig. 5b). In contrast to conservation within the coding regions, a total of 19 SNPs and three indels in the full-length 5′-flanking region were identified (Fig. 5c). To investigate the impact of variation in the 5′-flanking sequence on *ACBP3* expression, COM-C plants harboring *ACBP3pro (Col):: ACBP3::GFP* and COM-L plants harboring *ACBP3pro (Ler):: ACBP3::GFP* were used to complement *acbp3-2*. Stronger GFP signals were observed in anthers from COM-L transgenic Arabidopsis than COM-C (Fig. 5d). While anthers in COM-L flowers appear normal, those from COM-C were deformed (Fig. 5e). Further statistical analysis on anther lobes from L*er*-0, COM-L, COM-C and *acbp3-2* indicated that COM-C anthers possess more lobes than *acbp3-2* but fewer than L*er*-0 (Fig. 5f), suggesting partial recovery of retarded anther development in COM-C transgenic plants.

The 5′-flanking region of *ACBP3* in L*er*-0 and Col-0 react differently to SPL in EMSA and luciferase (LUC) assays

The 5′-flanking sequences of *ACBP3* in L*er*-0 and Col-0 were further analyzed *in silico* to investigate their differential effects on the *ACBP3* interactome (Fig. 6a). Within the high-variant region (−1343/−1193), three putative *cis*-elements including an AT~TATA Box, a 'Nameless' element and a CAAT Box were predicted by PLANTCARE (bioinformatics.psb.ugent.be/webtools/plantcare/html). Noticeably, multiple TA-repeats presented adjacent to the putative AT~TATA Box in *ACBP3* 5′-flanking sequences from Col-0 but not L*er*-0 (Fig. 6a). To identify the transcription factors (TFs) that bind these *cis*-elements, a literature search was conducted. TF SPL is known to regulate gene expression in early-staged anthers (Zheng *et al.*, 2021) and its mutation *spl* impair anther development (Yang *et al.*, 1999). However, its binding to specific *cis*-element (s) has not been reported. Therefore, EMSA experiments using recombinant SPL protein were performed to investigate the potential interaction of SPL with the 5′-flanking regions of *ACBP3* in L*er*-0 and Col-0. The results showed that SPL can specifically bind to Probe 1 from L*er*-0 but not Col-0 (Fig. 6b). In contrast, binding was not observed using Probes 2 and 3 from either L*er*-0 or Col-0 (Fig. 6b). These observations indicate that SPL binds specifically to the AT~TATA Box on the 5′-flanking region of *ACBP3* from L*er*-0. The binding of SPL to the 5′-flanking region of *ACBP3* from L*er*-0 was further verified using LUC assays (Fig. 6c–e). It was demonstrated that SPL can
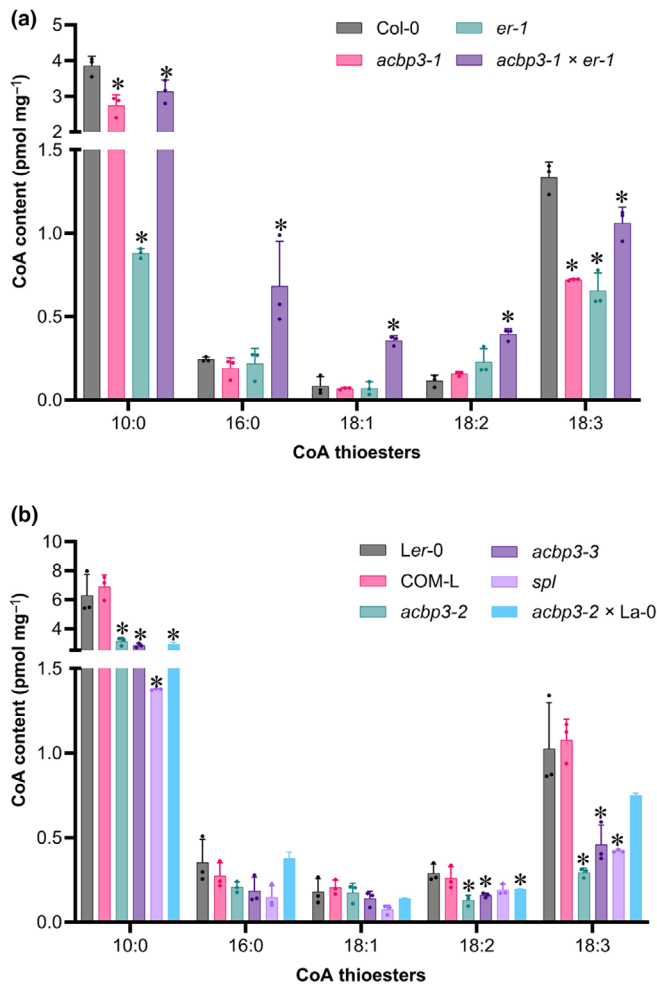
Fig. 3 Acyl-CoA profiles in anthers of *Arabidopsis thaliana* ecotypes Col-0 and L*er*-0. (a) High performance liquid chromatography (HPLC) analysis on acyl-CoA thioesters in anthers from Col-0, *acbp3*-1 and *er-1* mutants. Quantitative analyses were conducted on acyl-CoA thioesters (C10:0, C16:0, C18:1, C18:2 and C18:3-CoAs) from Arabidopsis anthers of Col-0, *acbp3*-1, *er-1* mutants and *acbp3*-1 × *er-1* plants. Values represent mean ± SE of measurements made on at least three independent batches of samples. The Student's *t*-test was performed to compare *acbp3*-1, *er-1* and *acbp3*-1 × *er-1* plants against the Col-0 control. Asterisks represent statistical differences in comparison to Col-0. *, $P < 0.05$. (b) HPLC analysis on acyl-CoA thioesters in anthers from L*er*-0, COM-L, *acbp3*-2, *acbp3*-3, *spl* mutants and *acbp3*-2 × La-0 plants. Quantitative analyses were conducted on acyl-CoA thioesters (C10:0, C16:0, C18:1, C18:2 and C18:3-CoAs) from Arabidopsis anthers of the aforementioned lines. Values represent mean ± SE of measurements made on three independent batches of samples. The Student's *t*-test was performed to compare the COM-L complement line, *acbp3*-2, *acbp3*-3, *spl* mutants and *acbp3*-2 × La-0 plants against the L*er*-0 control. Asterisks represent statistical differences in comparison to L*er*-0: *, $P < 0.05$.

activate the *ACBP3* promoter of L*er*-0 but not Col-0 (Fig. 6d,e). Additionally, real-time qRT-PCR analysis revealed that the expression of another four TFs involved in anther development were affected in *acbp3*-2 (Fig. S7), suggesting that knockout of *ACBP3* in L*er*-0 impacted the regulatory networks controlling anther development. Furthermore, downregulation of *ACBP3*

expression was observed in *spl* mutant flower buds (Fig. 6f), while overexpression of *SPL* restored normal levels of *ACBP3* expression in the SPL-overexpressing line *spl*-D in Col-0 (Li *et al.*, 2008).

Discussion

Polymorphism in the promoter of *ACBP3* in L*er*-0 genome distinguish its function from Col-0

In this study, the 5′-flanking sequences of *ACBP3* in L*er*-0 were found to differ from Col-0 by the presence of promoter polymorphism which regulated *ACBP3* expression and anther development (Figs 4, 5, S5). Higher expression of *ACBP3* in flower buds of L*er*-0 than Col-0 (Figs 4, S5) and greater *ACBP3* expression in those of L*er*-0 over other tested Arabidopsis ecotypes (Fig. S6) support the biological role of ACBP3 in L*er*-0 floral development. While the *ACBP3* cDNA sequences remain identical in Col-0 and L*er*-0, evidence of retarded sporocyte formation fully rescued in COM-L, but only partially in COM-C (Fig. 5), and of stronger GFP signals in COM-L than COM-C (Fig. 5d), suggests that proper *ACBP3* expression is crucial for anther development in L*er*-0 and abnormal expression adversely affects anther development (Figs 1, 2, 5).

Differences between the Col-0 and L*er*-0 genomes have been reported and include a 1.2-Mb large inversion on the short arm of chromosome 4 as well as differences between the *5S* rDNA clusters (Fransz *et al.*, 1998, 2000). In addition to the more than a hundred single-copy genes encountered only in the L*er*-0 genome, hundreds of copy-number polymorphisms, novel genes and single-copy orthologs occur in either L*er*-0 or Col-0 (Zapata *et al.*, 2016). Thus, it is not surprising that gene functions in L*er*-0 and Col-0 vary, because polymorphisms are known to cause phenotypic variations (Alonso-Blanco *et al.*, 2005). Noncoding polymorphism in the *FLOWERING LOCUS C* promoter was reported to influence gene expression enabling adaptation to cold winter temperatures in Arabidopsis plants (Zhu *et al.*, 2023).
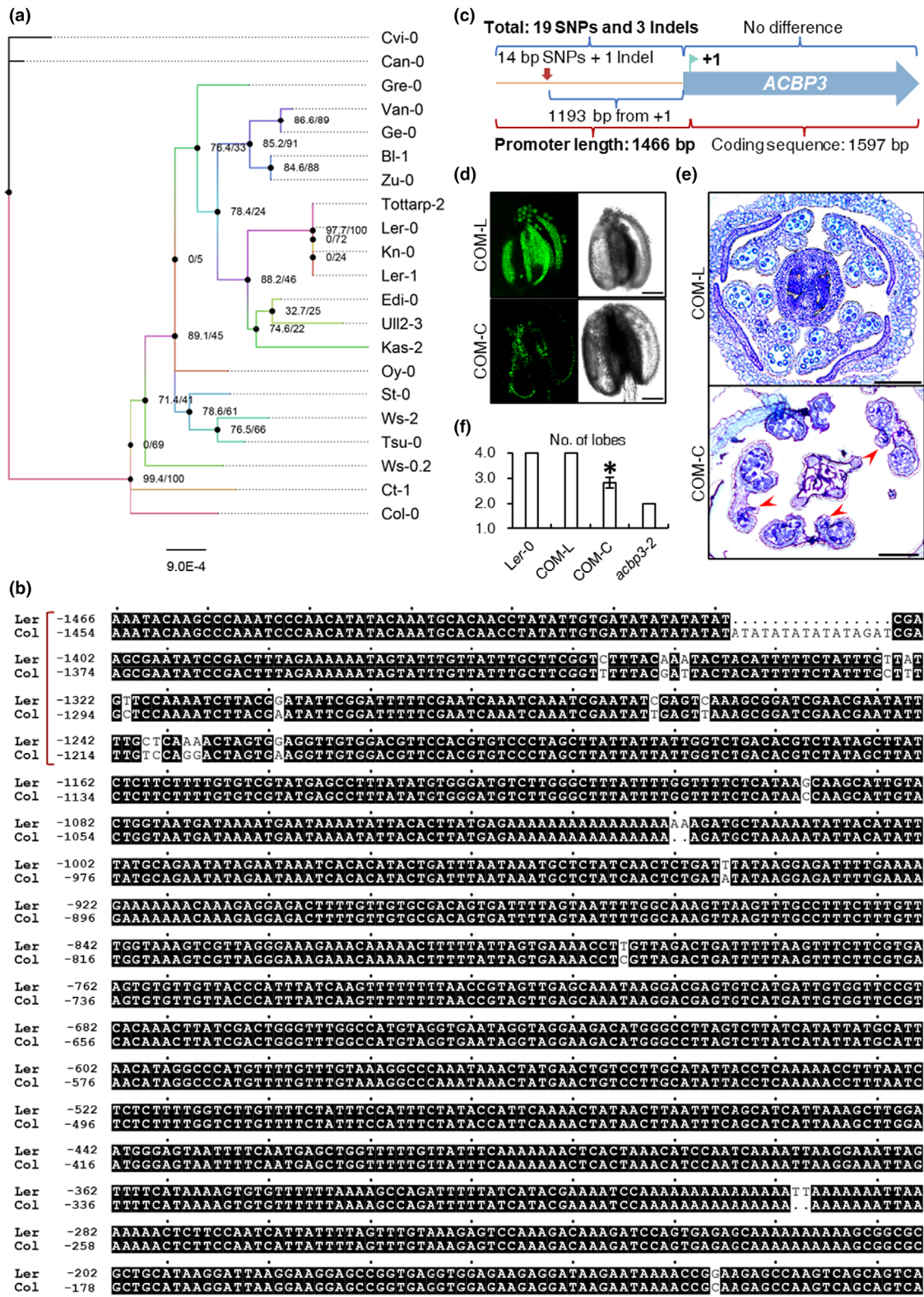
In Arabidopsis Landsberg, Col-0 and Ws-0, knockout of *ERECTA* affected the size of aboveground organs (van Zanten *et al.*, 2009). Similarly, ERECTA-like (ERL) proteins can act in ERECTA signaling during cell differentiation (Shpak *et al.*, 2003). Although single mutations in the *ERECTA* family genes have not been reported to impact anther development (Torii *et al.*, 1996), an *er-105 erl1-2 erl2-1* triple mutant displayed retarded anthers with missing lobes (Hord *et al.*, 2008), as well as abnormal cell differentiation in the ovule (Pillitteri *et al.*, 2007). The involvement of ERECTA in anther development, specifically its influence on the number of anther lobes, suggests a potential relationship between ACBP3 function in L*er*-0 and the ERECTA signaling pathway. This hypothesis is strongly supported by observations of the rescued anther phenotype in *acbp3*-2 × La-0 (Fig. 2g). However, the *acbp3*-2 *er-1* hybrid plant (*acbp3*-2 × *er-1*) in Fig. 2(e) and *acbp3*-1 × *er-1* (Fig. 2f) did not exhibit the same phenotype as *acbp3*-2 (Figs 1, 2c). This suggests that the distinct function of
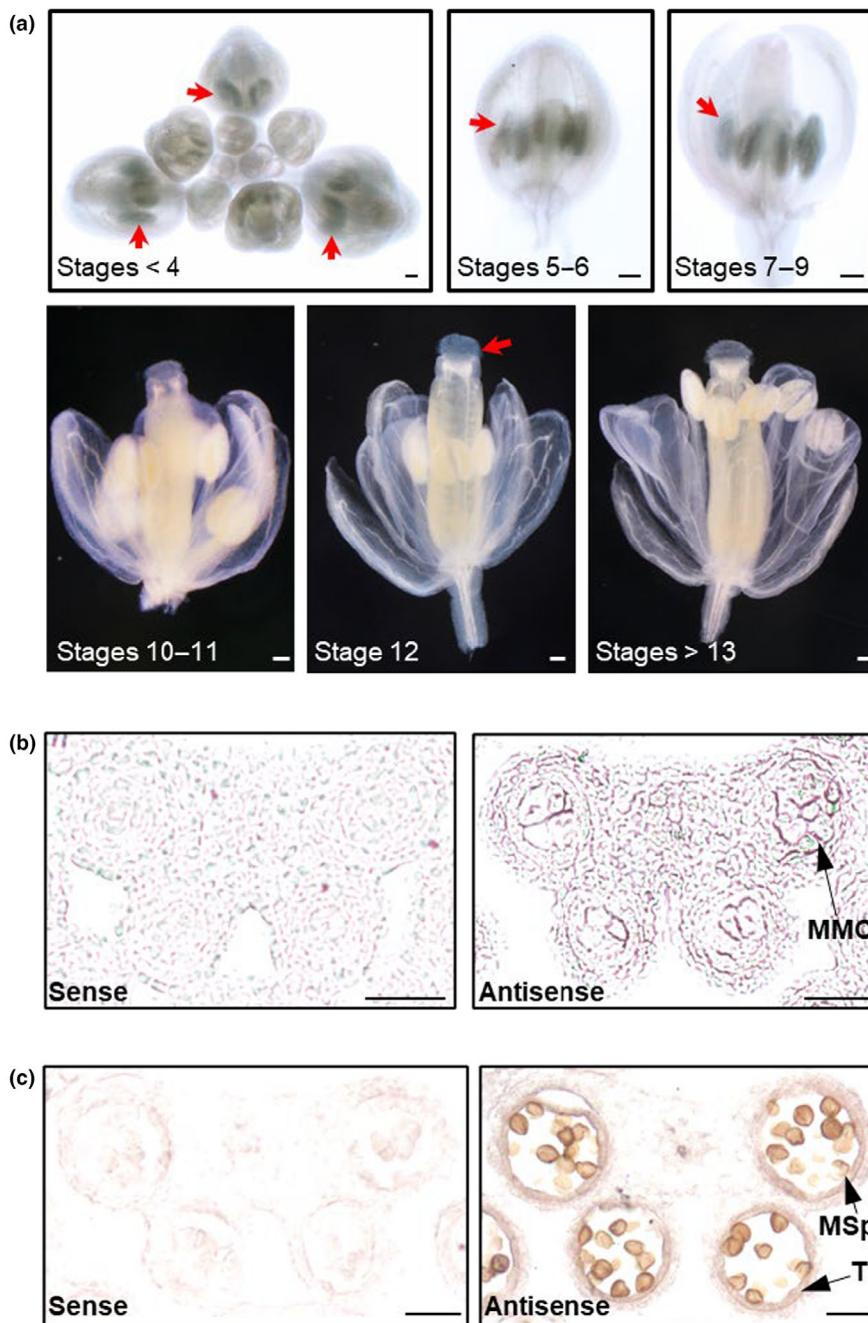
Fig. 4 Expression analysis of ACBP3 in *Arabidopsis thaliana* ecotype Ler-0. (a) Histochemical GUS staining was carried out on *ACBP3pro (Ler)::GUS* flowers containing staged 4–13 anthers, showing the expression of *ACBP3pro (Ler)::GUS* in anthers and stigmata of transgenic Arabidopsis Ler-0 flowers. Flowers containing anthers from stage < 4, stages 5–6, stages 7–9, stages 10–11, stage 12 and stage > 13 are presented. Red arrows indicate GUS signals seen in anthers until stage 8 and in stigma at stage 12. (b, c) RNA *in situ* assay of *ACBP3* expression in Ler-0 anthers at stages 4–5 and stages 7–9, respectively. The sense probe was used as a negative control on sections at the corresponding stage shown on the left, with antisense probe hybridization on the right. Bars: (a) 200 μm; (b, c) 20 μm. MMC, micro mother cells; MSp, microspores; T, tapetum.

Fig. 5 Variation in the *ACBP3* 5′-flanking sequence between *Arabidopsis thaliana* ecotypes Col-0 and Ler-0. (a) Representative Arabidopsis ecotypes from around the world for which *ACBP3* 5′-flanking sequences (data from https://1001genomes.org/) are compared. An evolutionary study was carried out on the −1343/−1193 region at the *ACBP3* 5′-flanking sequences aligned with the Muscle alignment program (Edgar, 2004a,b). Phylogenetic analysis was performed using maximum likelihood methods with W-IQ-Tree 1.6.12 (Trifinopoulos *et al.*, 2016). The SH-aLRT/bootstrap supporting value is displayed at each clade. The tree was visualized using FigTree 1.4.4. (b) Alignment of *ACBP3* 5′-flanking sequences from Ler-0 and Col-0. The numbering on the left is marked with respect to the transcription start site on *ACBP3* from each ecotype. The alignment was performed using ClustalW (Sievers *et al.*, 2011) and formatted in GeneDoc (Nicholas, 1997). Conserved nucleotides are shaded in black, and the region with frequent variation is indicated with a square bracket. (c) Diagram indicating presence of SNPs and indels on *ACBP3* 5′-flanking sequence in Ler-0 and Col-0. Major substitutions on the *ACBP3* 5′-flanking sequences coincide with the position marked by a red arrow. The number of variants is indicated with braces. Notably the most variations occur near −1193, where 14 SNPs and one indel map. In contrast, no variation was detected in the coding sequences. (d) *ACBP3pro (Ler)::ACBP3::GFP* and *ACBP3pro (Col)::ACBP3::GFP* were used to compliment the *acbp3-2* mutant in Ler-0, and they were designated as COM-L and COM-C respectively. Stronger GFP signals in anthers were detected from the COM-L than the COM-C transgenic Arabidopsis plants. (e) Normal anthers occur in COM-L flowers, in contrast to the deformed in COM-C. Deformed anther lobes are denoted indicated by arrowheads. Bars, 100 μm. (f) Statistical data on the number of anther lobes in Ler-0, COM-L, COM-C and *acbp3-2* (*n* = 16). Values represent mean ± SE. The asterisk represents statistical difference in comparison to both Ler-0 and *acbp3-2* (*P* < 0.01 using Student's *t*-test). The error bars for Ler-0, COM-L, and *acbp3-2* are zero.

(a)

(c) **Total: 19 SNPs and 3 Indels** — No difference
14 bp SNPs + 1 Indel → +1
ACBP3
1193 bp from +1
Promoter length: 1466 bp — Coding sequence: 1597 bp

(d)

(e)

(f) No. of lobes

(b)

ACBP3 in L*er*-0 is not solely attributed to the *er* mutation. A more intricate mechanism of action may involve additional members of the ERECTA family, such as ERL1 and ERL2. F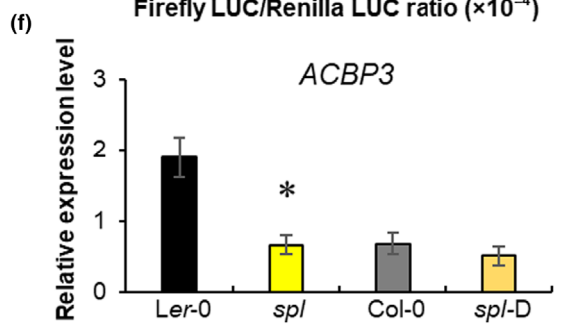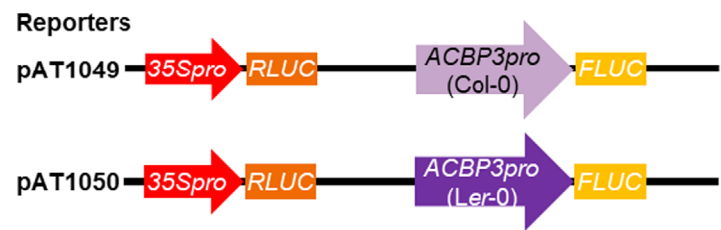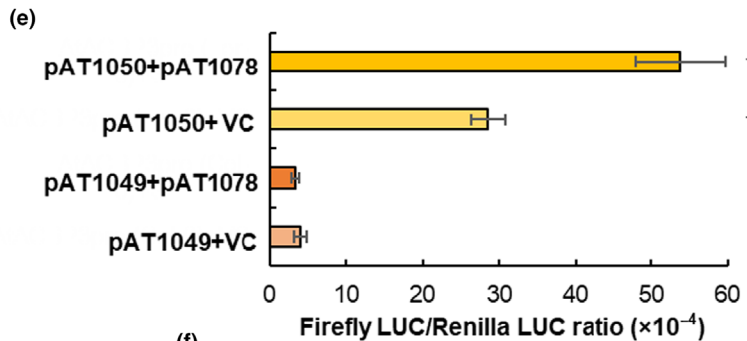urthermore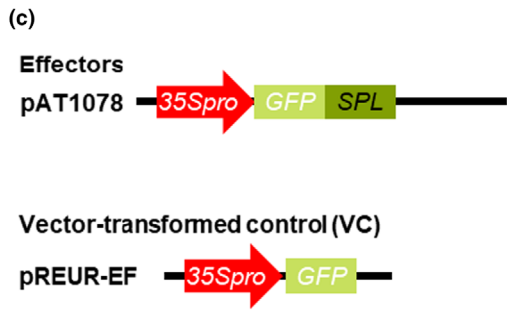, the absence of native ACBP3 expression in Col-0 anthers (Fig. S5) did not cause developmental defects (Fig. S2), indicating that there are differences in the regulatory network governing anther development between L*er*-0 and Col-0.

SPL binds to the 5′-flanking sequence of *ACBP3* in L*er*-0 and regulates floral development

The role of SPL in sporocyte formation is well established; the primary sporogenous cell layer in staged-3 anthers of *spl* failed to form

microsporocytes and vacuolated from stage 4 (Yang *et al.*, 1999). The observed defect for *acbp3-2* in sporocyte formation within adaxial lobes (Fig. 1) further supports the regulatory role of SPL on *ACBP3* expression in L*er*-0 anthers. In anthers, SPL is known to be phosphorylated by MITOGEN-ACTIVATED PROTEIN

Fig. (a) Alignment of *ACBP3* 5′-flanking sequences in L*er*-0 and Col-0 showing AT~TATA Box, Nameless, CAAT Box, and Probe 1, Probe 2, Probe 3 regions. (b) EMSA with Probe 1, Probe 2, Probe 3. (c) Effectors, Vector-transformed control (VC), and Reporters constructs. (d) Luciferase intensity in leaf. (e) Firefly LUC/Renilla LUC ratio (×10⁻⁴). (f) *ACBP3* relative expression level.
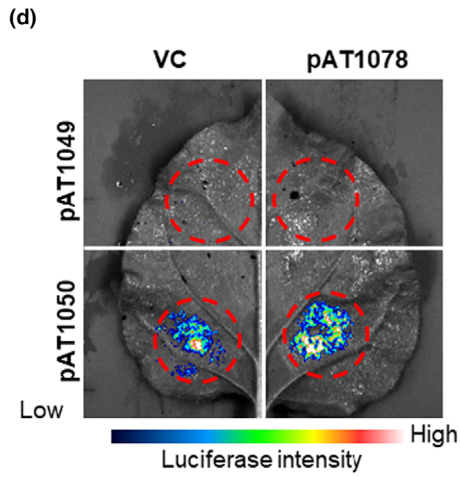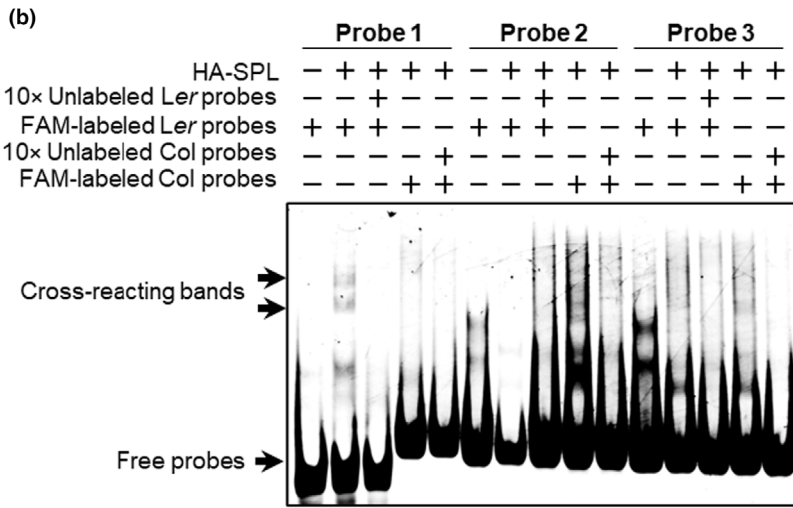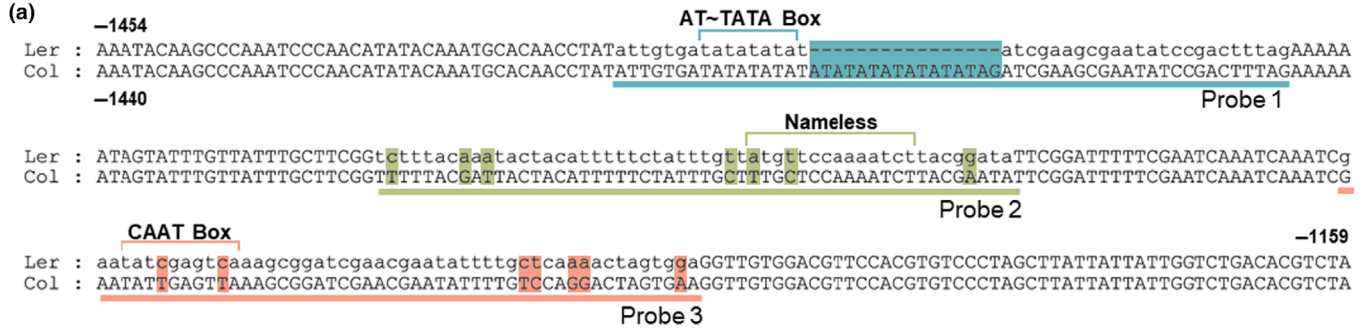
Fig. 6 A regulatory role for SPL on the *ACBP3* 5′-flanking sequence in *Arabidopsis thaliana* ecotype L*er*-0. (a) Alignment of the *ACBP3* 5′-flanking regions of L*er*-0 and Col-0 ranging from *c.* −1.4k to −1.1k. Sequence variations are highlighted in three colors (blue, green and orange). The putative *cis*-elements predicted by PLANTCARE (bioinformatics.psb.ugent.be/webtools/plantcare/html) are marked correspondingly to the adjacent sequence variations: AT~TATA Box in blue, 'Nameless' element in green and CAAT Box in orange. Probes for electrophoretic mobility shift assays (EMSAs) are denoted in the corresponding colors. (b) EMSA on recombinant proteins of SPOROCYTELESS (SPL) was carried out, as SPL was reported to regulate gene expression in early-staged anthers (Zheng *et al*., 2021). Double-stranded DNA probes were labeled with fluorescein amidites (FAM) at the 5′-end, while unlabeled probes were used in competing experiments. Cross-reacting bands are denoted with arrows. Symbols '−' indicate absence in the reaction, while '+' for presence in the reaction. (c) Schematic graph of constructs in LUC assays. Two constructs of reporters include the *ACBP3* 5′-flanking sequence from Col-0 (pAT1049) or L*er*-0 (pAT1050) cloned to drive the cDNA encoding firefly luciferase (FLUC). Plasmids pAT1049 and pAT1050 also contain the cDNA encoding *Renilla* luciferase (RLUC) driven by the *35S* promoter. Plasmid pREUR-EF acts as a vector-transformed control (VC). Plasmids pAT1078 is a pREUR-EF-derivative which harbors the *SPL* cDNA driven by the *35S* promoter. They were co-expressed in different combinations in *Nicotiana benthamiana* leaves. (d) The red circles of dashed lines indicate the area of injection. (e) Dual-luciferase assays showing the expression of FLUC normalized with RLUC. Values represent mean ± SE of measurements made on at least three independent biological replicates. The Student's *t*-test was performed between the effector and VC (*, $P < 0.05$). (f) qRT-PCR results show the expression of *ACBP3* in L*er*-0, *spl*, Col-0 and *spl*-D flower buds normalized against *ACTIN2*. Values represent mean ± SE of measurements made on at least three independent biological replicates. The Student's *t*-test was conducted to compare the readings between L*er*-0 and *spl*, as well as between Col-0 and *spl*-D (*, $P < 0.05$). No statistical difference of *ACBP3* expression from Col-0 and *spl*-D was detected.

KINASEs (MPKs) MPK3/6, and *mpk3/mpk6* mutants in Col-0 displayed defective adaxial but normal abaxial lobes (Zhao *et al*., 2017), similar to the *acbp3-2* mutant in L*er*-0 (Fig. 1). However, *SPL* expression was unaffected in *mpk3/mpk6* knockouts (Zhao *et al*., 2017). Given that SPL did not interact similarly with the *ACBP3* promoter from Col-0 or L*er*-0 (Fig. 6), it can be inferred that SPL function differs in these ecotypes. This study suggests that *SPL* likely regulates anther development through the activation of *ACBP3* expression in L*er*-0 (Fig. 6). The role of *SPL* is further supported by the downregulation of *ACBP3* expression in the *spl* mutant (Fig. 6f). In contrast, the overexpression of *SPL* did not affect *ACBP3* expression in Col-0 *spl*-D flower buds (Fig. 6f), indicating that SPL cannot effectively interact with the *ACBP3* promoter. Notably, significant differences within the −1343/−1193 region of the *ACBP3* promoter occurred between Col-0 and L*er*-0 (Fig. 5b). Furthermore, EMSA confirmed that SPL can only bind to the AT~TATA box in L*er*-0 (Fig. 6g), suggesting that the absence of multiple TA-repeats facilitated effective binding of SPL to the AT~TATA box on the *ACBP3* promoter in L*er*-0. Taken together, polymorphism within the *ACBP3* promoter altered the regulatory role of *SPL* on *ACBP3* expression, enabling its function in anther development.

It has been reported that knockout mutants of genes affecting *SPL* expression or those regulated by *SPL*, such as *BRASSINAZOLE-RESISTANT (BZR), TRYPTOPHAN AMINOTRANSFERASE OF ARABIDOPSIS 1 (TAA1), TRYPTOPHAN AMINOTRANSFERASE RELATED2 (TAR2)* and *TGA9/TGA10*, all exhibit similar phenotypes as the *spl* mutant (Murmu *et al*., 2010; Chen *et al*., 2019; Zheng *et al*., 2021), indicating their important roles in sporogenesis. In Arabidopsis, *taa1 tar2-1* and *taa2-2* mutants with markedly reduced *SPL* transcripts were impaired in anther locule formation (Zheng *et al*., 2021), while knockout mutants of six *BZR* genes barely express *SPL* and show abnormal sporocyte formation (Chen *et al*., 2019). Additionally, the double mutant of *TGA9* and *TGA10*, two basic leucine-zipper transcription factors downstream of *SPL*, exhibit normal abaxial anther lobes but variable or disorganized adaxial lobes (Murmu *et al*., 2010). The differential impact of *ACBP3* on abaxial and adaxial lobe

development observed in *acbp3-2* anthers in this study (Fig. 1) imply that *ACBP3* likely functions downstream of *SPL* in L*er*-0. Notably, *SPL* expression was upregulated in the *acbp3-2* mutant (Fig. S7). However, this upregulation of *SPL* failed to rescue the *acbp3-2* phenotype, suggesting that the roles of *ACBP3* and *SPL* in sporocyte formation do not completely overlap. The differential developmental progress observed between the abaxial and the adaxial lobes in *tga9 tga10* anthers indicates that the four lobes do not develop simultaneously (Murmu *et al*., 2010). The defective adaxial anther lobes accompanied by normal abaxial lobes in the *acbp3-2* mutant (Fig. 1) as observed in this study further support this phenomenon. Similar to the *spl* homozygous plants, which exhibit comparable overall morphology to L*er*-0 (Yang *et al*., 1999), *acbp3-2* did not impact vegetative growth (Fig. S3). However, unlike *spl* homozygous plants (Yang *et al*., 1999), *acbp3-2* did not exhibit delayed progression of senescence (Fig. S3). Conversely, when *SPL* was overexpressed in the *spl*-D line in Col-0 a curly-leaf phenotype resulted (Li *et al*., 2008), indicating that the role of SPL vary between Col-0 and L*er*-0.

ACBP expression and lipid composition affect plant reproduction

The findings of this study reinforce the significance of ACBPs in plant reproduction (Fadhli Hamdan *et al*., 2022) due to the adverse impact on anther development in L*er*-0 caused by knockout of ACBP3 (Figs 1, 2). Functions of other *ACBPs* such as *ACBP4, ACBP5* and *ACBP6* in reproduction have been established in *acbp4 acbp5 acbp6* since pollen grains of this triple mutant (Col-0) exhibit reduced and smaller oil bodies along with irregular exine arrangement (Hsiao *et al*., 2015). Furthermore, changes in phospholipid (PL) composition observed in *acbp4*, *acbp5* and *acbp6* mutants and changes in triacylglycerol (TAG) content in the *acbp6* seeds (Guo *et al*., 2019b) were accompanied by reduction in seed weight in the double and triple mutants (Hsiao *et al*., 2014), linking ACBP-mediated lipid metabolism to plant reproduction. Comparative sequence alignment analysis revealed numerous variations between Col-0 and L*er*-0 ecotypes

in both the promoter and coding regions for each of *ACBP4*, *ACBP5* and *ACBP6* (Table S2). Therefore, their expression profiles and biological functions may potentially differ between these two ecotypes.

ACBP-mediated lipid metabolism is attributed to its ability for lipid binding (Guo *et al.*, 2022). Recombinant rACBP3 exhibits binding specificity towards very-long-chain (VLC) acyl-CoA thioesters ($\geq$ C22) as well as phosphatidylethanolamine (PE), and plays crucial roles in VLC FA biosynthesis and PE-related autophagy (Xiao *et al.*, 2010; Hu *et al.*, 2018). Furthermore, it has been reported that PLs and VLC FAs are closely associated with floral development (Potocky *et al.*, 2003; Jung *et al.*, 2006; Jiang *et al.*, 2012; Nakamura *et al.*, 2014; Zhan *et al.*, 2018; Djanaguiraman *et al.*, 2019; Colin & Jaillais, 2020; Hernandez *et al.*, 2020). In L*er*-0 anthers, the *acbp3-2* mutant exhibits lower 10:0-, 18:2- and 18:3-CoA content while the *spl* mutants display reduction in 10:0- and 18:3-CoA (Fig. 3). This suggests that *SPL* operates upstream of *ACBP3* and may potentially regulate other genes involved in lipid metabolism, including a gene encoding a Lipid Transfer Protein family member, which showed altered expression in the *spl* mutant (Li *et al.*, 2008). Interestingly, similar to *spl* in L*er*-0, the *er-1* mutant in Col-0 exhibit reduction in 10:0- and 18:3-CoA content (Fig. 3). While *acbp3-1* × *er-1* also exhibits lower 10:0- and 18:3-CoA, it was elevated in 16:0-, 18:1- and 18:2-CoAs (Fig. 3a). In contrast, *acbp3-2* × La-0

plants demonstrated recovery in 18:3-CoA content in comparison to *acbp3-2* (Fig. 3b), supporting that ERECTA can affect acyl-CoA content in anthers. Noticeably, while the *acbp3-2* mutant did not exhibit higher levels of 16:0-, 18:1- and 18:2-CoA content compared to L*er*-0, the *acbp3-1* × *er-1* plants were elevated in these CoAs compared to *Col-0* (Fig. 3), which is consistent with differential anther morphology observed between *acbp3-1* × *er-1* and *acbp3-2* plants (Fig. 2). Taken together, ERECTA likely affects acyl-CoA content differently in Col-0 and La-0. Thus in L*er*-0, the role of *ACBP3* is associated with ERECTA, facilitated by genetic polymorphism in the regulatory region of *ACBP3* that enables its downstream function to be regulated by *SPL* (Fig. 5).

In summary, a new role for *ACBP3* in the development of anthers in Arabidopsis L*er*-0 is reported. As depicted in the proposed working model (Fig. 7), a comparison was made between the 5′-flanking sequences of *ACBP3* in Col-0 and L*er*-0. In L*er*-0, polymorphism in the promoter region of *ACBP3* from −1454 to −1159 (Fig. 6a) enabled the AT~TATA box function in L*er*-0 but not Col-0 (verified by EMSAs in Fig. 6). This change in the DNA sequence, in turn, altered the binding efficiency of the transcription factor SPL to the AT~TATA Box in the 5′-flanking region of *ACBP3* in L*er*-0 (Fig. 6b–e), which activated transcription (Fig. 4) and translation (Fig. 5) of *ACBP3* in L*er*-0 anthers. Ultimately, highly-expressed transcripts and proteins of ACBP3 in L*er*-0
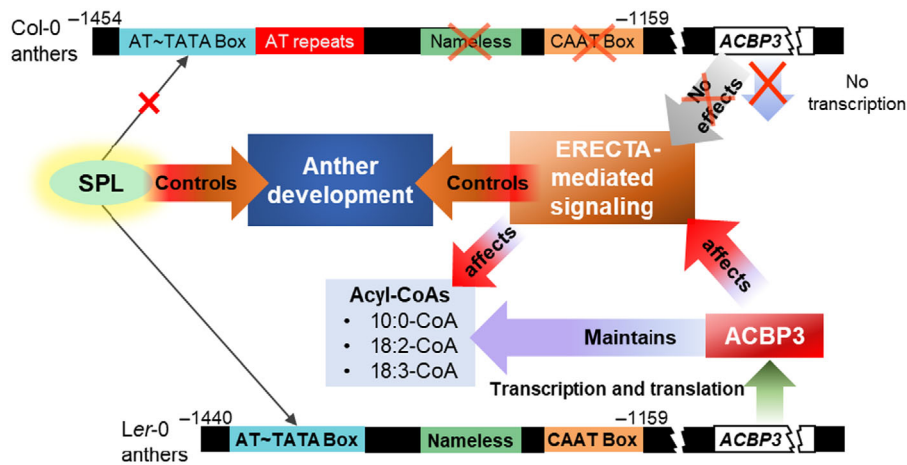
Fig. 7 Proposed model on the role of Arabidopsis *ACBP3* in anther development of *Arabidopsis thaliana* ecotypes Col-0 and L*er*-0. To test the hypothesis that the ERECTA (ER)-mediated signaling pathway is associated with the role of ACBP3, *acbp3-1* × *er-1* and *acbp3-2* × La-0 plants were generated and analyzed together with *acbp3* mutants by microscopy for anther morphology (Figs 1, 2) and high-performance liquid chromatography for lipid composition (Fig. 3). The role of ACBP3 in L*er*-0 anther development is enabled by promoter polymorphism, which allows *ACBP3* to function downstream of SPL. *ACBP3* expression in the anther of L*er*-0, but not in Col-0, is modulated by promoter polymorphism. Variation in the *ACBP3* 5′-flanking sequences ranging from *c.* −1.4k to −1.2k (not to scale) differs between Col-0 (top line) and L*er*-0 (bottom line). In anthers, the AT~TATA box, 'Nameless' element and CAAT Box are functional in L*er*-0 but not Col-0 (verified by EMSAs in Fig. 5). *ACBP3* is not expressed in Col-0 anthers (Supporting Information Fig. S5), and *ACBP3* did not function through the ER-mediated signaling pathway as supported by observations of normal anthers in *acbp3-1* × *er-1* (Fig. 2f). In L*er*-0, SPL interacts with the AT~TATA Box and activates *ACBP3* transcription (Fig. 5), influencing anther development and maintaining acyl-CoA homeostasis. In L*er*-0, mutations (a transposon mutation *acbp3-2* and a CRISPR mutation *acbp3-3*) in *ACBP3* adversely affect anther development (Figs 1, 2). ACBP3 function is related to the ER-mediated signaling pathway, as substantiated by the recovery of normal anthers in *acbp3-2* × La-0 plants (Fig. 2g). As ACBP3 has potential to maintain an acyl-CoA pool in anther development and ER could also affect anther acyl-CoA composition (Fig. 3), fatty acid composition was altered in *acbp3-2* and *acbp3-3*, with a shift in acyl-CoA composition specifically in 10:0-, 18:2- and 18:3-CoAs (Fig. 6). SPL, SPOROCYTELESS. Red crosses indicate disruption in function.

anthers maintain the anther acyl-CoA pool (Fig. 3) and promote anther development (Figs 1, 2) via the ERECTA-mediated signaling pathway. The impact of promoter polymorphisms on plant reproduction is illustrated through their effect on ACBP3 function in anther development. This study inspires further exploration of polymorphism functions in plants and ACBP-mediated lipid metabolism in reproduction. The impact on anther development has significant implications for food production as it regulates seed and fruit formation, thereby opening new avenues for enhancing agricultural productivity.

Acknowledgements

Competing interests

None declared.

Author contributions

M-LC, Z-HG and DZ designed the project. Z-HG performed most of the experiments. T-HH identified the *acbp3-2* mutant and performed FA analysis and *in vivo* pollination. MFH performed GUS histological stains. ML generated plasmid constructs. RW modified vectors. JX, S-CL, WL and JS analyzed data. Z-HG and M-LC wrote the paper with contribution from all authors.

ORCID

Mee-Len Chye https://orcid.org/0000-0003-3505-3674
Ze-Hua Guo https://orcid.org/0000-0002-7894-498X
Mohd Fadhli Hamdan https://orcid.org/0000-0001-7707-5770
Tai-Hua Hu https://orcid.org/0000-0002-4051-0027
Minghui Li https://orcid.org/0000-0002-2800-4842
Wanqi Liang https://orcid.org/0000-0002-9938-5793
Shiu-Cheung Lung https://orcid.org/0000-0002-6433-4988
Jianxin Shi https://orcid.org/0000-0002-7717-0863
Ruifeng Wang https://orcid.org/0009-0004-7452-4699
Jie Xu https://orcid.org/0000-0003-4574-4698
Dabing Zhang https://orcid.org/0000-0003-3181-9812

Data availability

All data and materials integral to this study are available within the article and the Supporting Information.

References

Abraham MC, Metheetrairut C, Irish VF. 2013. Natural variation identifies multiple loci controlling petal shape and size in *Arabidopsis thaliana. PLoS ONE* **8**: e56743.

AGI. 2000. Analysis of the genome sequence of the flowering plant *Arabidopsis thaliana. Nature* **408**: 796–815.

Alonso-Blanco C, Mendez-Vigo B, Koornneef M. 2005. From phenotypic to molecular polymorphisms involved in naturally occurring variation of plant development. *International Journal of Developmental Biology* **49**: 717–732.

Anisimova M, Gascuel O. 2006. Approximate likelihood-ratio test for branches: a fast, accurate, and powerful alternative. *Systematic Biology* **55**: 539–552.

Bray D, Bagu J, Koegler P. 1993. Comparison of hexamethyldisilazane (HMDS), Peldri II, and critical-point drying methods for scanning electron microscopy of biological specimens. *Microscopy Research and Technique* **26**: 489–495.

Burton M, Rose TM, Faergeman NJ, Knudsen J. 2005. Evolution of the acyl-CoA binding protein (ACBP). *The Biochemical Journal* **392**: 299–307.

Carvalho AP, Malcata FX. 2005. Preparation of fatty acid methyl esters for gas-chromatographic analysis of marine lipids: insight studies. *Journal of Agricultural and Food Chemistry* **53**: 5049–5059.

Chen L-G, Gao Z, Zhao Z, Liu X, Li Y, Zhang Y, Liu X, Sun Y, Tang W. 2019. BZR1 family transcription factors function redundantly and indispensably in BR signaling but exhibit BRI1-independent function in regulating anther development in *Arabidopsis. Molecular Plant* **12**: 1408–1415.

Chen M-X, Hu T-H, Xue Y, Zhu F-Y, Du Z-Y, Lo C, Chye M-L. 2018. Arabidopsis acyl-coenzyme-A-binding protein ACBP1 interacts with AREB1 and mediates salt and osmotic signaling in seed germination and seedling growth. *Environmental and Experimental Botany* **156**: 130–140.

Chen Q-F, Xiao S, Chye M-L. 2008. Overexpression of the Arabidopsis 10-kilodalton acyl-coenzyme A-binding protein ACBP6 enhances freezing tolerance. *Plant Physiology* **148**: 304–315.

Chen QF, Xiao S, Qi W, Mishra G, Ma J, Wang M, Chye M-L. 2010. The Arabidopsis *acbp1acbp2* double mutant lacking acyl-CoA-binding proteins ACBP1 and ACBP2 is embryo lethal. *New Phytologist* **186**: 843–855.

Chye M-L. 1998. Arabidopsis cDNA encoding a membrane-associated protein with an acyl-CoA binding domain. *Plant Molecular Biology* **38**: 827–838.

Clough SJ, Bent AF. 1998. Floral dip: a simplified method for *Agrobacterium*-mediated transformation of *Arabidopsis thaliana. The Plant Journal* **16**: 735–743.

Colin LA, Jaillais Y. 2020. Phospholipids across scales: lipid patterns and plant development. *Current Opinion in Plant Biology* **53**: 1–9.

Crawford BC, Yanofsky MF. 2011. *HALF FILLED* promotes reproductive tract development and fertilization efficiency in *Arabidopsis thaliana. Development* **138**: 2999–3009.

Djanaguiraman M, Schapaugh W, Fritschi F, Nguyen H, Prasad PVV. 2019. Reproductive success of soybean (*Glycine max* L. Merril) cultivars and exotic lines under high daytime temperature. *Plant, Cell & Environment* **42**: 321–336.

Du Z-Y, Arias T, Meng W, Chye M-L. 2016. Plant acyl-CoA-binding proteins: an emerging family involved in plant development and stress responses. *Progress in Lipid Research* **63**: 165–181.

Du Z-Y, Chen M-X, Chen Q-F, Xiao S, Chye M-L. 2013a. Arabidopsis acyl-CoA-binding protein ACBP1 participates in the regulation of seed germination and seedling development. *The Plant Journal* **74**: 294–309.

Du Z-Y, Chen M-X, Chen Q-F, Xiao S, Chye M-L. 2013b. Overexpression of Arabidopsis acyl-CoA-binding protein ACBP2 enhances drought tolerance. *Plant, Cell & Environment* **36**: 300–314.

Du Z-Y, Xiao S, Chen Q-F, Chye M-L. 2010. Depletion of the membrane-associated acyl-coenzyme A-binding protein ACBP1 enhances the ability of cold acclimation in Arabidopsis. *Plant Physiology* **152**: 1585–1597.

Edgar RC. 2004a. MUSCLE: a multiple sequence alignment method with reduced time and space complexity. *BMC Bioinformatics* **5**: 113.

Edgar RC. 2004b. MUSCLE: multiple sequence alignment with high accuracy and high throughput. *Nucleic Acids Research* **32**: 1792–1797.

Fadhli Hamdan M, Lung S-C, Guo Z-H, Chye M-L. 2022. Roles of acyl-CoA-binding proteins in plant reproduction. *Journal of Experimental Botany* **73**: 2918–2936.

Felsenstein J. 1985. Confidence limits on phylogenies: an approach using the bootstrap. *Evolution* **39**: 783–791.

Fransz P, Armstrong S, Alonso-blanco C, Fischer TC, Torres-ruiz RA, Jones G. 1998. Cytogenetics for the model system *Arabidopsis thaliana. The Plant Journal* **13**: 867–876.

Fransz PF, Armstrong S, de Jong JH, Parnell LD, van Drunen C, Dean C, Zabel P, Bisseling T, Jones GH. 2000. Integrated cytogenetic map of chromosome arm 4S of *A. thaliana*: structural organization of heterochromatic knob and centromere region. *Cell* **100**: 367–376.

Gao W, Xiao S, Li H-Y, Tsao S-W, Chye M-L. 2009. *Arabidopsis thaliana* acyl-CoA-binding protein ACBP2 interacts with heavy-metal-binding farnesylated protein AtFP6. *New Phytologist* **181**: 89–102.

Guo Z-H, Haslam RP, Michaelson LV, Yeung EC, Lung SC, Napier JA, Chye M-L. 2019a. The overexpression of rice ACYL-COA-BINDING PROTEIN 2 increases grain size and bran oil content in transgenic rice. *The Plant Journal* **100**: 1132–1147.

Guo Z-H, Lung SC, Fadhli Hamdan M, Chye M-L. 2022. Interactions between plant lipid-binding proteins and their ligands. *Progress in Lipid Research* **86**: 101156.

Guo Z-H, Pogancev G, Meng W, Du Z-Y, Liao P, Zhang R, Chye M-L. 2021. The overexpression of rice ACYL-COA-BINDING PROTEIN4 improves salinity tolerance in transgenic rice. *Environmental and Experimental Botany* **183**: 104349.

Guo Z-H, Ye Z-W, Haslam RP, Michaelson LV, Napier JA, Chye M-L. 2019b. Arabidopsis cytosolic acyl-CoA-binding proteins function in determining seed oil composition. *Plant Direct* **3**: e00182.

Haslam RP, Larson TR. 2021. Techniques for the measurement of molecular species of acyl-CoA in plants and microalgae. In: Bartels D, Dormann P, eds. *Plant lipids: methods and protocols.* New York, NY, USA: Springer, 203–218.

Hellens RP, Allan AC, Friel EN, Bolitho K, Grafton K, Templeton MD, Karunairetnam S, Gleave AP, Laing WA. 2005. Transient expression vectors for functional genomics, quantification of promoter activity and RNA silencing in plants. *Plant Methods* **1**: 13.

Hernandez ML, Lima-Cabello E, Alche JD, Martinez-Rivas JM, Castro AJ. 2020. Lipid composition and associated gene expression patterns during pollen germination and pollen tube growth in olive (*Olea europaea* L.). *Plant & Cell Physiology* **61**: 1348–1364.

Hord CLH, Sun Y-J, Pillitteri LJ, Torii KU, Wang H, Zhang S, Ma H. 2008. Regulation of *Arabidopsis* early anther development by the mitogen-activated protein kinases, MPK3 and MPK6, and the ERECTA and related receptor-like kinases. *Molecular Plant* **1**: 645–658.

Hsiao AS, Haslam RP, Michaelson LV, Liao P, Chen QF, Sooriyaarachchi S, Mowbray SL, Napier JA, Tanner JA, Chye M-L. 2014. Arabidopsis cytosolic acyl-CoA-binding proteins ACBP4, ACBP5 and ACBP6 have overlapping but distinct roles in seed development. *Bioscience Reports* **34**: e00165.

Hsiao AS, Yeung EC, Ye Z-W, Chye M-L. 2015. The Arabidopsis cytosolic acyl-CoA-binding proteins play combinatory roles in pollen development. *Plant & Cell Physiology* **56**: 322–333.

Hu T-H, Lung S-C, Ye Z-W, Chye M-L. 2018. Depletion of Arabidopsis ACYL-COA-BINDING PROTEIN3 affects fatty acid composition in the phloem. *Frontiers in Plant Science* **9**: 2.

Jefferson RA, Kavanagh TA, Bevan MW. 1987. GUS fusions: beta-glucuronidase as a sensitive and versatile gene fusion marker in higher plants. *EMBO Journal* **6**: 3901–3907.

Jiang J, Zhang Z, Cao J. 2012. Pollen wall development: the associated enzymes and metabolic pathways. *Plant Biology* **15**: 249–263.

Jung KH, Han MJ, Lee DY, Lee YS, Schreiber L, Franke R, Faust A, Yephremov A, Saedler H, Kim YW et al. 2006. Wax-deficient *anther1* is involved in cuticle and wax production in rice anther walls and is required for pollen development. *Plant Cell* **18**: 3015–3032.

Kouchi H, Hata S. 1993. Isolation and characterization of novel nodulin cDNAs representing genes expressed at early stages of soybean nodule development. *Molecular & General Genetics* **238**: 106–119.

Kowalski SP, Lan TH, Feldmann KA, Paterson AH. 1994. QTL mapping of naturally-occurring variation in flowering time of *Arabidopsis thaliana. Molecular & General Genetics* **245**: 548–555.

Kunkel BN. 1996. A useful weed put to work: genetic analysis of disease resistance in *Arabidopsis thaliana. Trends in Genetics* **12**: 63–69.

Lease KA, Lau NY, Schuster RA, Torii KU, Walker JC. 2001. Receptor serine/threonine protein kinases in signalling: analysis of the erecta receptor-like kinase of *Arabidopsis thaliana. New Phytologist* **151**: 133–143.

Leung KC, Li HY, Xiao S, Tse MH, Chye M-L. 2006. *Arabidopsis* ACBP3 is an extracellularly targeted acyl-CoA-binding protein. *Planta* **223**: 871–881.

Li G, Liang W, Zhang X, Ren H, Hu J, Bennett MJ, Zhang D. 2014. Rice actin-binding protein RMD is a key link in the auxin–actin regulatory loop that controls cell growth. *Proceedings of the National Academy of Sciences, USA* **111**: 10377–10382.

Li LC, Qin GJ, Tsuge T, Hou XH, Ding MY, Aoyama T, Oka A, Chen Z, Gu H, Zhao Y. 2008. *SPOROCYTELESS* modulates *YUCCA* expression to regulate the development of lateral organs in Arabidopsis. *New Phytologist* **179**: 751–764.

Li N, Zhang D-S, Liu H-S, Yin C-S, Li X-X, Liang W-Q, Yuan Z, Xu B, Chu H-W, Wang J. 2006. The rice tapetum degeneration retardation gene is required for tapetum degradation and anther development. *Plant Cell* **18**: 2999–3014.

Liao P, Chen Q-F, Chye M-L. 2014. Transgenic Arabidopsis flowers overexpressing acyl-CoA-binding protein ACBP6 are freezing tolerant. *Plant & Cell Physiology* **55**: 1055–1071.

Liu W-H, Wang R-F, Liu W-L, Xu J. 2020. Effects of different regulatory elements and their combinations on transient expressions of exogenous proteins in *Nicotiana benthamiana. Biotechnology Bulletin* **36**: 62–71.

Lung S-C, Chye M-L. 2016. Deciphering the roles of acyl-CoA-binding proteins in plant cells. *Protoplasma* **253**: 1177–1195.

Lung S-C, Lai SH, Wang H, Zhang X, Liu A, Guo Z-H, Lam H-M, Chye M-L. 2022. Oxylipin signaling in salt-stressed soybean is modulated by ligand-dependent interaction of Class II acyl-CoA-binding proteins with lipoxygenase. *Plant Cell* **34**: 1117–1143.

Murashige T, Skoog F. 1962. A revised medium for rapid growth and bio assays with tobacco tissue cultures. *Physiologia Plantarum* **15**: 473–497.

Murmu J, Bush MJ, DeLong C, Li S, Xu M, Khan M, Malcolmson C, Fobert PR, Zachgo S, Hepworth SR. 2010. Arabidopsis basic leucine-zipper transcription factors TGA9 and TGA10 interact with floral glutaredoxins ROXY1 and ROXY2 and are redundantly required for anther development. *Plant Physiology* **154**: 1492–1504.

Nakamura Y, Andrés F, Kanehara K, Liu Y-C, Dörmann P, Coupland G. 2014. Arabidopsis florigen FT binds to diurnally oscillating phospholipids that accelerate flowering. *Nature Communications* **5**: 1–7.

Nicholas KB. 1997. GeneDoc: analysis and visualization of genetic variation. *Embnew News* **4**: 14.

Panthapulakkal Narayanan S, Liao P, Taylor PWJ, Lo C, Chye M-L. 2019. Overexpression of a monocot acyl-CoA-binding protein confers broad-spectrum pathogen protection in a dicot. *Proteomics* **19**: 1800368.

Pillitteri LJ, Bemis SM, Shpak ED, Torii KU. 2007. Haploinsufficiency after successive loss of signaling reveals a role for ERECTA-family genes in Arabidopsis ovule development. *Development* **134**: 3099–3109.

Potocky M, Elias M, Profotova B, Novotna Z, Valentova O, Zarsky V. 2003. Phosphatidic acid produced by phospholipase D is required for tobacco pollen tube growth. *Planta* **217**: 122–130.

Rédei GP. 1962. Supervital mutants of Arabidopsis. *Genetics* **47**: 443–460.

Sanders PM, Bui AQ, Weterings K, McIntire K, Hsu Y-C, Lee PY, Truong MT, Beals T, Goldberg R. 1999. Anther developmental defects in *Arabidopsis thaliana* male-sterile mutants. *Sexual Plant Reproduction* **11**: 297–322.

Schmalenbach I, Zhang L, Ryngajllo M, Jiménez-Gómez JM. 2014. Functional analysis of the Landsberg *erecta* allele of *FRIGIDA*. *BMC Plant Biology* **14**: 218.

Schneider CA, Rasband WS, Eliceiri KW. 2012. NIH Image to ImageJ: 25 years of image analysis. *Nature Methods* **9**: 671–675.

Schwarz G. 1978. Estimating the dimension of a model. *The Annals of Statistics* **6**: 461–464.

Shpak ED, Lakeman MB, Torii KU. 2003. Dominant-negative receptor uncovers redundancy in the Arabidopsis ERECTA leucine-rich repeat receptor–like kinase signaling pathway that regulates organ shape. *Plant Cell* **15**: 1095–1110.

Sievers F, Wilm A, Dineen D, Gibson TJ, Karplus K, Li W, Lopez R, McWilliam H, Remmert M, Söding J *et al*. 2011. Fast, scalable generation of high-quality protein multiple sequence alignments using Clustal Omega. *Molecular Systems Biology* **7**: 539.

Tao J, Liang W, An G, Zhang D. 2018. OsMADS6 controls flower development by activating rice FACTOR OF DNA METHYLATION LIKE1. *Plant Physiology* **177**: 713–727.

Torii KU, Mitsukawa N, Oosumi T, Matsuura Y, Yokoyama R, Whittier RF, Komeda Y. 1996. The Arabidopsis *ERECTA* gene encodes a putative receptor protein kinase with extracellular leucine-rich repeats. *Plant Cell* **8**: 735–746.

Trifinopoulos J, Nguyen L-T, von Haeseler A, Minh BQ. 2016. W-IQ-Tree: a fast online phylogenetic tool for maximum likelihood analysis. *Nucleic Acids Research* **44**: W232–W235.

Xiao S, Chye M-L. 2011a. New roles for acyl-CoA-binding proteins (ACBPs) in plant development, stress responses and lipid metabolism. *Progress in Lipid Research* **50**: 141–151.

Xiao S, Chye M-L. 2011b. Overexpression of Arabidopsis ACBP3 enhances NPR1-dependent plant resistance to *Pseudomonas syringe* pv *tomato* DC3000. *Plant Physiology* **156**: 2069–2081.

Xiao S, Gao W, Chen Q-F, Chan SW, Zheng S-X, Ma JY, Wang MF, Welti R, Chye M-L. 2010. Overexpression of Arabidopsis acyl-CoA binding protein ACBP3 promotes starvation-induced and age-dependent leaf senescence. *Plant Cell* **22**: 1463–1482.

Yang W-C, Ye D, Xu J, Sundaresan V. 1999. The *SPOROCYTELESS* gene of *Arabidopsis* is required for initiation of sporogenesis and encodes a novel nuclear protein. *Genes & Development* **13**: 2108–2117.

Ye Z-W, Chye M-L. 2016. Plant cytosolic acyl-CoA-binding proteins. *Lipids* **51**: 1–13.

Ye Z-W, Lung S-C, Hu T-H, Chen Q-F, Suen Y-L, Wang M, Hoffmann-Benning S, Yeung E, Chye M-L. 2016. Arabidopsis acyl-CoA-binding protein ACBP6 localizes in the phloem and affects jasmonate composition. *Plant Molecular Biology* **92**: 1–14.

Ye Z-W, Xu J, Shi J, Zhang D, Chye M-L. 2017. Kelch-motif containing acyl-CoA binding proteins AtACBP4 and AtACBP5 are differentially expressed and function in floral lipid metabolism. *Plant Molecular Biology* **93**: 209–225.

Yeung EC, Chan CK. 2015. The glycol methacrylate embedding resins – Technovit 7100 and 8100. In: Yeung ECT, Stasolla C, Sumner MJ, Huang BQ, eds. *Plant microtechniques and protocols*. Berlin, Germany: Springer, 67–82.

van Zanten M, Snoek LB, Proveniers MCG, Peeters AJM. 2009. The many functions of ERECTA. *Trends in Plant Science* **14**: 214–218.

Zapata L, Ding J, Willing E-M, Hartwig B, Bezdan D, Jiao W-B, Patel V, James GV, Koornneef M, Ossowski S. 2016. Chromosome-level assembly of *Arabidopsis thaliana* Ler reveals the extent of translocation and inversion polymorphisms. *Proceedings of the National Academy of Sciences, USA* **113**: E4052–E4060.

Zhan H, Xiong H, Wang S, Yang ZN. 2018. Anther endothecium-derived very-long-chain fatty acids facilitate pollen hydration in Arabidopsis. *Molecular Plant* **11**: 1101–1104.

Zhao F, Zheng Y-F, Zeng T, Sun R, Yang J-Y, Li Y, Ren D-T, Ma H, Xu Z-H, Bai S-N. 2017. Phosphorylation of SPOROCYTELESS/NOZZLE by the MPK3/6 kinase is required for anther development. *Plant Physiology* **173**: 2265–2277.

Zheng S-X, Xiao S, Chye M-L. 2012. The gene encoding Arabidopsis acyl-CoA-binding protein 3 is pathogen inducible and subject to circadian regulation. *Journal of Experimental Botany* **63**: 2985–3000.

Zheng Y, Wang D, Ye S, Chen W, Li G, Xu Z, Bai S, Zhao F. 2021. Auxin guides germ-cell specification in *Arabidopsis* anthers. *Proceedings of the National Academy of Sciences, USA* **118**: e2101492118.

Zhu P, Schon M, Questa J, Nodine M, Dean C. 2023. Causal role of a promoter polymorphism in natural variation of the Arabidopsis floral repressor gene *FLC*. *Current Biology* **33**: 4381–4391.

Supporting Information

Additional Supporting Information may be found online in the Supporting Information section at the end of the article.

Fig. S1 Characterization of the *acbp3* mutants in *Arabidopsis thaliana* ecotype Ler-0.

Fig. S2 Scanning electron microscopy (SEM) images of anthers from *acbp3* mutants in *Arabidopsis thaliana* ecotypes Col-0 and Ler-0.

Fig. S3 Comparison of inflorescence, rosette and stem between *acbp3* and wild-type *Arabidopsis thaliana* ecotypes Col-0 and Ler-0.

Fig. S4 Knockout of ACBP3 alters fatty acid (FA) composition in *Arabidopsis thaliana* ecotype Ler-0 flower buds.

Fig. S5 *ACBP3* is expressed in female organs of wild-type *Arabidopsis thaliana* ecotype Col-0.

Fig. S6 *ACBP3* expression in flower buds from various *Arabidopsis thaliana* ecotypes.

Fig. S7 qRT-PCR assay using flower bud total mRNA show changes in the expression of five transcription factors (TFs) in *acbp3-2* in comparison to wild-type *Arabidopsis thaliana* ecotype Ler-0.

Table S1 Oligomers used in this study.

Table S2 Variations in genomic DNA sequence of Arabidopsis *ACBPs* from *Arabidopsis thaliana* ecotypes Col-0 and Ler-0.

Please note: Wiley is not responsible for the content or functionality of any Supporting Information supplied by the authors. Any queries (other than missing material) should be directed to the *New Phytologist* Central Office.